NUMERICAL APPROACH TO THE LONDON EQUATION OF SUPERCONDUCTIVITY

NICOLÁS BARNAFI, IGNACIO LABARCA-FIGUEROA, AND CARLOS ROMÁN

Abstract. In this work, we propose a general discretization strategy for solving the London equation for type-II superconductors in the whole space $\mathbb{R}^3$. To compute the magnetic field H_0, we reformulate the problem for the magnetic potential as a transmission problem and discretize it through a nonstandard Finite Element–Boundary Element (FEM–BEM) coupling. This formulation accounts for the unbounded exterior domain as well as the interior domain without introducing an artificial truncation.

We then compute the vector field B_0, which arises from the Helmholtz–Hodge decomposition of the magnetic potential in the superconducting sample. This field enters the isoflux problem, which identifies the curves along which vortex nucleation first becomes energetically favorable in the Ginzburg–Landau (GL) model of superconductivity. We recast the equations for B_0 using the mixed formulation of Kikuchi, in which the divergence-free constraint is imposed weakly, and discretize the resulting problem using a classical $H(\text{curl})$-conforming Finite Elements (FE) discretization.

We validate our discretization strategy through convergence tests and conclude with an application to the isoflux problem. For a ball under a constant applied magnetic field, the unique maximizer is the diameter aligned with the field. For ellipsoids under a constant applied magnetic field aligned with their major axis, our computations provide numerical evidence of a different behavior in sufficiently elongated, cigar-shaped geometries: off-axis competitors reminiscent of U-shaped vortex configurations attain a larger isoflux ratio than the major axis. Since the major axis is therefore not a maximizer, any off-axis maximizer generates, by rotational symmetry, a continuous family of equivalent configurations, implying non-uniqueness and the presence of a degenerate rotational direction in the isoflux problem.

Acronyms.

Date: July 29, 2026.

2020 *Mathematics Subject Classification.* 35Q56,65N22,82D55,65N30,78M15.

Key words and phrases. London equation, isoflux problem, First critical field, Finite Elements method, Boundary Elements method.

Funding information: ANID FONDECYT 1231593, Centro de Modelamiento Matemático, Proyecto Basal FB210005.

FE: Finite Elements 1

FEM: Finite Element Method 4

FEM–BEM: Finite Element–Boundary Element 1

GL: Ginzburg–Landau 1

1. Introduction

1.1. **Problem and background.** The analysis of the first critical field H_{c_1} in the three-dimensional magnetic GL model of superconductivity leads to the study of the well-known *London equation* for the magnetic field H_0,

$$\operatorname{curl}\operatorname{curl}(H_0 - H_{0,\mathrm{ex}}) + H_0 \mathbf{1}_\Omega = 0 \quad \text{in } \mathbb{R}^3, \tag{1}$$

supplemented by the conditions $\lim_{|x|\to\infty} |H_0 - H_{0,\mathrm{ex}}| = 0$ and $[H_0 - H_{0,\mathrm{ex}}]_{\partial\Omega} = 0$. Here, Ω represents the material sample, which we assume to be a bounded, simply connected subset of $\mathbb{R}^3$ with C^2 boundary, and $\mathbf{1}_\Omega$ denotes its indicator function. The applied magnetic field is assumed to have the form $H_{\mathrm{ex}} \coloneqq h_{\mathrm{ex}} H_{0,\mathrm{ex}}$, where $H_{0,\mathrm{ex}}$ is normalized so that $\|H_{0,\mathrm{ex}}\|_{L^\infty(\mathbb{R}^3)} = 1$ and represents its direction, while $h_{\mathrm{ex}} > 0$ is a tunable parameter representing its intensity. Throughout the paper, we refer to $H_{0,\mathrm{ex}}$ as the normalized applied magnetic field. Moreover, $[\,\cdot\,]_{\partial\Omega}$ denotes the jump across $\partial\Omega$. Both H_0 and $H_{0,\mathrm{ex}}$ are divergence-free vector fields, in view of their magnetic field structure.

Superconductivity was first discovered in 1911 by Heike Kamerlingh Onnes, who observed that mercury's electrical resistance vanished abruptly at very low temperatures. This discovery emerged from his pioneering studies of matter at low temperatures, work that earned him the Nobel Prize in Physics in 1913. The experimental breakthrough revealed a new state of matter but initially lacked a theoretical explanation. The London equation, originally formulated in terms of the superconducting current by Fritz and Heinz London in [LL35], provided the first phenomenological framework for the Meissner effect, namely, the expulsion of magnetic fields from the interior of a superconductor below its critical temperature, with penetration only over a characteristic length scale. This phenomenon is one of the most striking features of superconductivity and underlies magnetic levitation.

The London equation for the magnetic field (1) naturally arises in the GL framework. The GL theory [GL50] deepened the phenomenological description of superconductivity by introducing an order parameter and a variational framework. Although not microscopic, it has proven to be an extraordinarily powerful theory, successfully accounting for most macroscopic features of superconductors. Moreover, it can be rigorously derived [FHSS12] as the limiting form of the microscopic Bardeen–Cooper–Schrieffer (BCS) theory [BCS57], in which superconductivity is explained by the formation of Cooper pairs of electrons.

In type-II superconductors, sufficiently strong applied magnetic fields can penetrate the sample through quantized vortex lines. In three dimensions, these vortices take the form of filaments, around which the superconducting current circulates and along whose cores superconductivity is locally lost. The first critical field H_{c_1} marks the transition, at the level of global minimizers of the GL functional, from configurations without vortex filaments for

$h_{\mathrm{ex}} < H_{c_1}$ to configurations containing vortex filaments for $h_{\mathrm{ex}} > H_{c_1}$. Equation (1) plays a central role in the computation of H_{c_1} and in determining where vortex filaments first nucleate within the sample.

In [Rom19], the last author showed that

$$H_{c_1} = \frac{1}{2\,\mathrm{R}_0}|\log\varepsilon| + O(\log|\log\varepsilon|) \quad \text{as } \varepsilon \to 0, \tag{2}$$

together with a strong characterization of minimizers both below and above H_{c_1}. Here:

- $\varepsilon > 0$ is the inverse of the *GL parameter* $\kappa = \lambda/\xi$, where λ is the London penetration depth, the characteristic length over which magnetic fields penetrate the superconductor, and ξ is the coherence length, the characteristic length over which the superconducting order parameter varies. In this notation, type-II superconductors correspond to $0 < \varepsilon < \sqrt{2}$, while the asymptotic regime $\varepsilon \to 0$ describes extreme type-II superconductivity;
- the constant R_0 corresponds to the value of the *isoflux problem*, that is,
$$\mathrm{R}_0 = \sup_{\Gamma \in X} \mathrm{R}(\Gamma) \coloneqq \sup_{\Gamma \in X} \frac{1}{|\Gamma|}\int_\Gamma B_0 \cdot d\ell,$$
where X is the set of curves in $\overline{\Omega}$ that do not self-intersect and that are either loops contained in Ω or have two distinct endpoints on $\partial\Omega$. The vector field B_0 is directly related to the magnetic field H_0 solving (1) and is obtained by solving
$$\begin{cases} \operatorname{curl}\operatorname{curl} B_0 &= H_0 & \text{in } \Omega \\ \operatorname{div} B_0 &= 0 & \text{in } \Omega \\ B_0 \times \nu &= 0 & \text{on } \partial\Omega, \end{cases} \tag{3}$$
where hereafter ν denotes the outer unit normal to $\partial\Omega$. Even though we will not make use of it, it is worth mentioning that it is not hard to prove that B_0 and $H_{0,\mathrm{ex}} - H_0$ differ only by the gradient of a harmonic function.

The last author, together with E. Sandier and S. Serfaty, [RSS23, RSS25] strengthened the expansion (2) to

$$H_{c_1} = \frac{1}{2\,\mathrm{R}_0}\left(|\log\varepsilon| + C_{\Omega,\Gamma_0}\right) + o(1) \quad \text{as } \varepsilon \to 0, \tag{4}$$

when R_0 is attained by a unique curve Γ_0 that is non-degenerate in a suitable sense. Here, C_{Ω,Γ_0} is a constant that depends on Ω and Γ_0. In addition, above H_{c_1}, vortex filaments appear and exhibit a sequence of transitions, with vortex lines appearing one by one as the intensity of the applied magnetic field is increased: after passing H_{c_1}, there is one vortex; then, after increasing the applied field by an increment of order $\log|\log\varepsilon|$, a second vortex line appears, and so on. These vortex lines accumulate near Γ_0 and, after a suitable horizontal blow-up around Γ_0, they minimize a next-order energy in the asymptotic limit $\varepsilon \to 0$.

The only case thus far in which Γ_0 has been identified is when Ω is a ball and $H_{0,\mathrm{ex}}$ is the constant vector field given by the unit vector in the z-direction. In this setting, an explicit solution of the London equation, and hence an explicit expression for H_0, was first obtained in [Lon50]. Using this explicit solution, Alama, Bronsard, and Montero subsequently identified

B_0 in [ABM06] and showed that

$$H_{c_1} \leq \frac{1}{2\,\mathrm{R}_0} |\log \varepsilon| + o(|\log \varepsilon|) \quad \text{as } \varepsilon \to 0,$$

in this special situation. This was later strengthened to

$$H_{c_1} = \frac{1}{2\,\mathrm{R}_0} |\log \varepsilon| + o(|\log \varepsilon|) \quad \text{as } \varepsilon \to 0,$$

by Baldo, Jerrard, Orlandi, and Soner in [BJOS13], for arbitrary domains and applied magnetic fields, together with a weak characterization of the behavior of minimizers both below and above H_{c_1}, later refined into the sharper expansions (2) and (4), as established in the works cited above.

Obtaining an analytical solution to the London equation (1) for general domains and normalized applied fields remains a challenging problem. The main objective of this paper is therefore to numerically solve (1) under fairly general hypotheses on both Ω and $H_{0,\mathrm{ex}}$. The determination of B_0, which depends on the solution of the London equation, presents similar analytical difficulties. In view of the key role played by B_0 in the nucleation of vortex filaments in the magnetic GL model of superconductivity, we also aim to compute it numerically.

1.2. **Approximation strategy.** For problems posed on bounded domains, a widely used discretization technique is the Finite Element Method (FEM); see [Mon03, BS08]. A triangulation of the domain leads to a finite-dimensional approximation in which local polynomial spaces are used as an ansatz for the solution. In the case of Maxwell's equations, this approach is a standard tool in computational electromagnetism; see [Hip02a].

The London equation (1), however, couples the interior field to an exterior field defined on an unbounded domain. We account for the exterior field without discretizing the exterior domain by representing it through boundary integral operators acting on suitable trace data. This approach is standard for exterior problems in computational electromagnetics, particularly in the context of time-harmonic Maxwell equations; see, for example, [Hip02b, BHvPS03, SS11]. The resulting discretization scheme is known as the Boundary Element Method (BEM).

This boundary integral representation naturally leads to a coupled FEM–BEM formulation of the London equation (1), viewed as a transmission problem between the bounded interior domain and the unbounded exterior domain. Such a formulation requires the discretization only of the field in the interior domain and of suitable data on its boundary. Previous numerical studies of London-type models for finite superconductors have typically incorporated the vacuum field through Biot–Savart or Green-function integral formulations, especially for thin films and SQUID-type devices [Bra94, Bra96, KKGS03, CB05]. To the best of our knowledge, a three-dimensional $H(\mathrm{curl})$-conforming FEM–BEM transmission discretization of the bulk London problem in the full exterior domain has not previously been analyzed in this form.

We next turn to the numerical determination of B_0, using the field H_0 computed through the coupled FEM–BEM formulation described above. More precisely, B_0 is recovered by solving the constrained curl–curl problem (3), with H_0 as its source term. To handle the divergence-free constraint, we introduce a scalar Lagrange multiplier and formulate (3) as a mixed saddle-point problem, following the approach of Kikuchi [Kik87]. The well-posedness of this formulation follows directly from the de Rham complex associated with the standard differential operators. Furthermore, the theory of FE Exterior Calculus [Arn18] ensures that standard conforming FE schemes yield stable and convergent discretizations. We therefore adopt this strategy and establish a Strang-type estimate that guarantees the approximability of B_0 when the numerically computed field H_0, rather than the exact solution of (1), is used as the source term in (3).

The overall solution strategy that we propose, based on the sequential computation of H_0 and B_0, falls within standard FEM and BEM frameworks and therefore allows for an efficient and scalable set of algorithms. This involves the use of preconditioned iterative methods for each linear problem, more specifically GMRES [SS86] with blockwise Algebraic Multigrid (AMG) iterations [Hac85]. We implement this strategy using the FEniCS library [ABH+15] and the PETSc interface [B+19] for the numerical linear algebra. The BEM block is naturally well-conditioned due to the use of second-kind Boundary Integral Equations (BIEs) with a stable duality pairing in trace spaces [BC07]. Implementation follows through an extension of the Bempp-cl library [BS21] to the setting of static Maxwell boundary integral operators.

1.3. **Application to the isoflux problem.** We conclude by using the computed field B_0 to provide numerical evidence of a qualitative change in the isoflux problem. For a ball under a constant normalized applied magnetic field, the unique maximizer is the diameter aligned with the field. We then consider ellipsoids whose major axis is aligned with the applied field, so that the major axis plays the corresponding role. Our computations suggest that this curve ceases to be optimal when the ellipsoid is sufficiently elongated. Indeed, we construct off-axis competitors with a larger isoflux ratio, whose geometry points toward the emergence of U-shaped vortex configurations. These competitors lie within two-dimensional sections of the ellipsoid determined by planes containing the major axis, and remain entirely on one side of it. For a representative ellipsoid, Figure 1 shows the competitor with the largest isoflux ratio within the family considered in our computations, illustrating the U-shaped geometry toward which the maximizing curves appear to evolve.

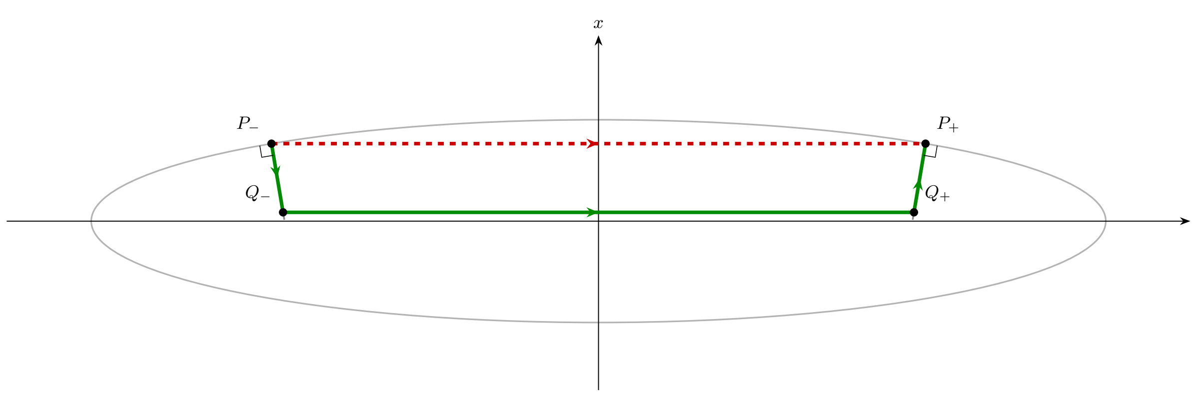

FIGURE 1. Off-axis competitor attaining the largest isoflux ratio within the family considered, with an isoflux ratio larger than that of the major axis of the ellipsoid and a geometry resembling a U-shaped vortex configuration. See Section 7 for details.

The rotational symmetry of the ellipsoid has two distinct consequences. First, rotations of an off-axis configuration generate a continuous family of equivalent configurations, suggesting non-uniqueness in the isoflux problem. Second, the continuous rotational invariance introduces a degenerate direction along this family.

Consequently, the refined analysis of [RSS23, RSS25], where uniqueness and non-degeneracy of the maximizing curve of the isoflux problem are essential assumptions, cannot be applied. This suggests a qualitatively different vortex-nucleation scenario, governed by a degenerate family of competing curves rather than by a single distinguished filament, and points toward the possible emergence of U-shaped configurations analogous to those observed in rotating Bose–Einstein condensates [RBD02, AD03]; see Section 7 for details.

Plan of the paper. The remainder of the paper is organized as follows. In Section 2, which can be read independently of the rest of the paper, we derive the London equation from the GL model. Section 3 introduces the functional setting and the trace spaces used throughout the paper. In Section 4, we reformulate the London equation as a transmission problem suitable for FEM–BEM coupling. Section 5 develops the numerical approximation of H_0 and B_0 and establishes the convergence of the overall formulation. In Section 6, we present numerical tests assessing the convergence of the proposed method and validate it against the explicit solution available for a ball under a uniform normalized applied field. In Section 7, we use the computed field B_0 to explore the isoflux problem in ellipsoidal domains and provide numerical evidence that, for sufficiently elongated geometries, the major axis ceases to be optimal in favor of off-axis competitors resembling U-shaped vortex configurations. The explicit solution used in the numerical validation is presented in Appendix A, while the layer potentials, boundary integral operators, representation formula, and Calderón equations required for the treatment of the exterior problem are collected in Appendix B.

2. Derivation of the London equation

In this section, following the presentation in [Rom19], we recall how the London equation arises from the GL model of superconductivity. In an applied magnetic field and at fixed temperature below the critical one, the state of a superconducting sample is modeled by the energy functional

$$GL_\varepsilon(u, A) \coloneqq \frac{1}{2}\int_\Omega |\nabla_A u|^2 + \frac{1}{2\varepsilon^2}(1-|u|^2)^2 + \frac{1}{2}\int_{\mathbb{R}^3} |\operatorname{curl} A - H_{\mathrm{ex}}|^2. \tag{5}$$

Here, $u : \Omega \to \mathbb{C}$ is the *order parameter*. Its squared modulus $|u|^2$ represents the local density of Cooper pairs, the paired-electron states that underlie superconductivity in BCS theory, and thus encodes the local superconducting state. $A : \mathbb{R}^3 \to \mathbb{R}^3$ is the electromagnetic vector potential generating the induced magnetic field $H \coloneqq \operatorname{curl} A$. ∇_A denotes the covariant derivative, defined as $\nabla - iA$.

The GL model is a $\mathbb{U}(1)$ gauge theory, meaning that all physically meaningful quantities are invariant under the gauge transformations

$$u \mapsto ue^{i\phi} \quad \text{and} \quad A \mapsto A + \nabla\phi,$$

where ϕ is any sufficiently regular real-valued function. In what follows, we will work on the divergence-free gauge, that is, we assume without loss of generality that $\operatorname{div} A = 0$ in $\mathbb{R}^3$.

Since $\operatorname{div} H_{\mathrm{ex}} = 0$ in $\mathbb{R}^3$, in accordance with the nonexistence of magnetic monopoles in Maxwell's theory of electromagnetism, we deduce that there exists a vector potential $A_{\mathrm{ex}} \in H^1_{\mathrm{loc}}(\mathbb{R}^3, \mathbb{R}^3)$ such that

$$\operatorname{curl} A_{\mathrm{ex}} = H_{\mathrm{ex}} \quad \text{and} \quad \operatorname{div} A_{\mathrm{ex}} = 0 \text{ in } \mathbb{R}^3.$$

We also define $A_{0,\mathrm{ex}} \coloneqq h_{\mathrm{ex}}^{-1} A_{\mathrm{ex}}$.

One of the contributions of [Rom19] is the construction of a precise approximation of the *Meissner state*, that is, the unique (modulo gauge-invariance) solution of the GL equations without vortex filaments. This solution corresponds to the global minimizer of (5) below the first critical field. The approximating configuration, which is roughly obtained by minimizing (5) among configurations such that $|u| = 1$, is given by

$$(e^{ih_{\mathrm{ex}}\phi_0}, h_{\mathrm{ex}} A_0), \tag{6}$$

where A_0 is the unique minimizer in $[A_{0,\mathrm{ex}} + \dot{H}^1_{\mathrm{div}=0}(\mathbb{R}^3, \mathbb{R}^3)]$ of the energy functional

$$J(A) \coloneqq \frac{1}{2} \int_\Omega |A - \nabla \phi_A|^2 + \frac{1}{2} \int_{\mathbb{R}^3} |\operatorname{curl}(A - A_{0,\mathrm{ex}})|^2,$$

where $\dot{H}^1_{\mathrm{div}=0}(\mathbb{R}^3, \mathbb{R}^3)$ denotes the subspace of divergence-free vector fields in the homogeneous Sobolev space $\dot{H}^1(\mathbb{R}^3, \mathbb{R}^3)$, and ϕ_A is the unique solution in $H^1(\Omega)$ with zero average, that is, $\int_\Omega \phi_A = 0$, of the elliptic problem

$$\begin{cases} \operatorname{div}(A - \nabla\phi_A) &= 0 \quad \text{in } \Omega \\ (A - \nabla\phi_A) \cdot \nu &= 0 \quad \text{on } \partial\Omega \end{cases} \iff \begin{cases} \Delta\phi_A &= 0 \quad \text{in } \Omega \\ \nabla\phi_A \cdot \nu &= A \cdot \nu \quad \text{on } \partial\Omega, \end{cases}$$

where the equivalence comes from $\operatorname{div} A = 0$ in $\mathbb{R}^3$. In view of the Helmholtz–Hodge decomposition, the preceding system yields

$$A - \nabla\phi_A = \operatorname{curl} B_A \quad \text{in } \Omega \tag{7}$$

for a unique vector field B_A satisfying $\operatorname{div} B_A = 0$ in Ω and $B_A \times \nu = 0$ on $\partial\Omega$. The phase appearing in (6) is then defined by $\phi_0 \coloneqq \phi_{A_0}$. We also set $B_0 = B_{A_0}$.

The Euler–Lagrange equation solved by the minimizer A_0 of J is given by

$$\operatorname{curl}\operatorname{curl}(A_0 - A_{0,\mathrm{ex}}) + \mathbf{1}_\Omega \operatorname{curl} B_0 = 0 \quad \text{in } \mathbb{R}^3. \tag{8}$$

Let $H_0 \coloneqq \operatorname{curl} A_0$. By taking the curl of (8) in both Ω and $\mathbb{R}^3 \setminus \overline{\Omega}$, we obtain the London equation for the magnetic field (1). The condition $\lim_{|x|\to\infty} |H_0 - H_{0,\mathrm{ex}}| = 0$ follows from the fact that $A_0 \in [A_{0,\mathrm{ex}} + \dot{H}^1_{\mathrm{div}=0}(\mathbb{R}^3, \mathbb{R}^3)]$.

Let us now derive the boundary condition that H_0 satisfies on $\partial\Omega$, that is,

$$[H_0 - H_{0,\mathrm{ex}}]_{\partial\Omega} = 0. \tag{9}$$

For this, we let X be an arbitrary smooth vector field with compact support in $\mathbb{R}^3$. Testing (8) against X and integrating by parts the first term, we find

$$\int_{\mathbb{R}^3} (H_0 - H_{0,\mathrm{ex}}) \cdot \operatorname{curl} X + \int_\Omega \operatorname{curl} B_0 \cdot X = 0. \tag{10}$$

Doing the same with $X\mathbf{1}_\Omega$, we obtain

$$\int_\Omega (H_0 - H_{0,\mathrm{ex}}) \cdot \operatorname{curl} X - \int_{\partial\Omega} ((H_0 - H_{0,\mathrm{ex}}) \times \nu) \cdot X + \int_\Omega \operatorname{curl} B_0 \cdot X = 0. \tag{11}$$

Analogously, now using $X\mathbf{1}_{\mathbb{R}^3\setminus\Omega}$ as test vector field, we find

$$\int_{\mathbb{R}^3\setminus\Omega}(H_0 - H_{0,\mathrm{ex}}) \cdot \operatorname{curl} X - \int_{\partial(\mathbb{R}^3\setminus\Omega)} ((H_0 - H_{0,\mathrm{ex}}) \times (-\nu)) \cdot X = 0. \tag{12}$$

Summing (11) and (12), and using (10), we deduce that

$$\int_{\partial\Omega} ([H_0 - H_{0,\mathrm{ex}}]_{\partial\Omega} \times \nu) \cdot X = 0,$$

and hence $[H_0 - H_{0,\mathrm{ex}}]_{\partial\Omega} \times \nu = 0$.

On the other hand, we have that

$$\operatorname{div}(H_0 - H_{0,\mathrm{ex}}) = 0 \quad \text{in } \mathbb{R}^3.$$

Arguing similarly as above, one finds that $[H_0 - H_{0,\mathrm{ex}}]_{\partial\Omega} \cdot \nu = 0$, and therefore (9) holds.

Finally, we observe that (3) follows by taking the curl of (8) in Ω and combining the resulting equation with the restriction of (1) to Ω.

3. Functional setting

We rely on the standard Sobolev space $H^1(\Omega)$ and its natural trace space, denoted by

$$H^{1/2}(\partial\Omega) \coloneqq \gamma_D\big(H^1(\Omega)\big),$$

where γ_D is the Dirichlet trace operator. The dual space of $H^{1/2}(\partial\Omega)$ is denoted by $H^{-1/2}(\partial\Omega)$.

The vector-valued Sobolev spaces used throughout this work are

$$\begin{aligned}
H(\operatorname{curl}, \Omega) &\coloneqq \left\{U \in [L^2(\Omega)]^3 \ : \ \operatorname{curl} U \in [L^2(\Omega)]^3\right\},\\
H(\operatorname{curl}^2, \Omega) &\coloneqq \{U \in H(\operatorname{curl}, \Omega) \ : \ \operatorname{curl} U \in H(\operatorname{curl}, \Omega)\},\\
H(\operatorname{div}, \Omega) &\coloneqq \left\{U \in [L^2(\Omega)]^3 \ : \ \operatorname{div} U \in L^2(\Omega)\right\}.
\end{aligned}$$

We define the interior trace operators by

$$\begin{aligned}
\gamma_\tau^- U &\coloneqq U \times \nu, & \gamma_\tau^- &: H(\operatorname{curl}, \Omega) \longrightarrow H^{-1/2}(\operatorname{div}_{\partial\Omega}, \partial\Omega),\\
\gamma_N^- U &\coloneqq \operatorname{curl} U \times \nu, & \gamma_N^- &: H(\operatorname{curl}^2, \Omega) \longrightarrow H^{-1/2}(\operatorname{div}_{\partial\Omega}, \partial\Omega),\\
\gamma_\nu^- U &\coloneqq U \cdot \nu, & \gamma_\nu^- &: H(\operatorname{div}, \Omega) \longrightarrow H^{-1/2}(\partial\Omega),
\end{aligned}$$

where

$$H^{-1/2}(\operatorname{div}_{\partial\Omega}, \partial\Omega) \coloneqq \left\{\lambda \in H_\times^{-1/2}(\partial\Omega) \ : \ \operatorname{div}_{\partial\Omega} \lambda \in H^{-1/2}(\partial\Omega)\right\}$$

is the natural tangential Sobolev space, as defined in [BCS02], and $\operatorname{div}_{\partial\Omega}$ is the surface divergence operator. Here, we write $\mathbf{H}_\times^{-1/2}(\partial\Omega)$ for the dual space of

$$\mathbf{H}_\times^{1/2}(\partial\Omega) \coloneqq \gamma_\tau([H^1(\Omega)]^3),$$

as in [BCS02, Section 2] and [BHvPS03, Definition 1].

The exterior trace operators γ_τ^+, γ_N^+, and γ_ν^+ are defined analogously on $H(\operatorname{curl}, \mathbb{R}^3 \setminus \overline{\Omega})$, $H(\operatorname{curl}^2, \mathbb{R}^3 \setminus \overline{\Omega})$, and $H(\operatorname{div}, \mathbb{R}^3 \setminus \overline{\Omega})$, respectively.

For a vector field U for which the corresponding interior and exterior traces are well-defined, we denote the jumps across $\partial\Omega$ by $[\gamma_\tau U]$, $[\gamma_N U]$, and $[\gamma_\nu U]$.

4. Transmission formulation of the London equation

To reformulate the London equation (1) in a form suitable for the coupled FEM–BEM formulation developed below, we introduce an auxiliary vector field U_0. In the interior domain, the purpose of this reformulation is to work directly with the divergence-free component of A_0 arising from the Helmholtz–Hodge decomposition. Indeed, by (7),

$$A_0 - \nabla\phi_0 = \operatorname{curl} B_0 \quad \text{in } \Omega.$$

Thus, replacing A_0 by $A_0 - \nabla\phi_0$ allows us to write the interior equation directly in terms of $\operatorname{curl} B_0$, without explicitly retaining the gradient component $\nabla\phi_0$.

In the exterior domain, we instead start from $A_0 - A_{0,\mathrm{ex}}$ and introduce an additional gradient correction. More precisely, we define ψ as the unique harmonic extension of $\phi_0|_{\partial\Omega}$ to the exterior domain that vanishes at infinity:

$$\begin{cases} \Delta\psi &= 0 & \text{in } \mathbb{R}^3 \setminus \overline{\Omega}, \\ \psi &= \phi_0 & \text{on } \partial\Omega, \\ \lim\limits_{|x|\to\infty} \psi(x) &= 0. \end{cases}$$

In particular, $\nabla\psi \in L^2(\mathbb{R}^3 \setminus \overline{\Omega})$. Since ψ and ϕ_0 have the same trace on $\partial\Omega$, their tangential derivatives agree there, and hence

$$(\nabla\phi_0 - \nabla\psi) \times \nu = 0 \quad \text{on } \partial\Omega. \tag{13}$$

We then define

$$U_0 \coloneqq \begin{cases} A_0 - \nabla\phi_0 & \text{in } \Omega, \\ A_0 - A_{0,\mathrm{ex}} - \nabla\psi & \text{in } \mathbb{R}^3 \setminus \overline{\Omega}. \end{cases} \tag{14}$$

The exterior component of U_0 decays at infinity. Moreover, since $\operatorname{curl}\nabla\psi = 0$, the gradient correction does not alter the relation between $\operatorname{curl} U_0$ and the magnetic field or the exterior equation satisfied by U_0. In fact, the magnetic field H_0 is recovered from U_0 through

$$\operatorname{curl} U_0 = H_0 \quad \text{in } \Omega, \qquad \operatorname{curl} U_0 = H_0 - H_{0,\mathrm{ex}} \quad \text{in } \mathbb{R}^3 \setminus \overline{\Omega}. \tag{15}$$

The asymmetric definition of U_0 in (14) is deliberate. In the interior domain, we do not subtract $A_{0,\mathrm{ex}}$, as doing so would require incorporating the Helmholtz–Hodge decomposition of this additional term into the formulation. With the present choice, the interior equation has the right-hand side

$$\mathbf{f}_{\mathrm{ex}} \coloneqq \operatorname{curl}\operatorname{curl} A_{0,\mathrm{ex}} = \operatorname{curl} H_{0,\mathrm{ex}},$$

which vanishes, in particular, when the normalized applied magnetic field is constant. In the exterior domain, by contrast, subtracting $A_{0,\mathrm{ex}}$ produces a homogeneous equation. Using the Euler–Lagrange equation (8), we therefore obtain

$$\operatorname{curl}\operatorname{curl} U_0 = 0 \quad \text{in } \mathbb{R}^3 \setminus \overline{\Omega}, \qquad \operatorname{curl}\operatorname{curl} U_0 + U_0 = \mathbf{f}_{\mathrm{ex}} \quad \text{in } \Omega.$$

It remains to determine the transmission conditions on $\partial\Omega$. From (13), we obtain

$$\begin{aligned} [\gamma_\tau U_0] &= (A_0 - A_{0,\mathrm{ex}} - \nabla\psi) \times \nu - (A_0 - \nabla\phi_0) \times \nu \\ &= -\gamma_\tau A_{0,\mathrm{ex}} \quad \text{on } \partial\Omega. \end{aligned}$$

Moreover, (15) and $[H_0 - H_{0,\mathrm{ex}}]_{\partial\Omega} = 0$ give

$$\begin{aligned}[\gamma_N U_0] &= ((H_0 - H_{0,\mathrm{ex}}) - H_0) \times \nu \\ &= -H_{0,\mathrm{ex}} \times \nu \\ &= -\gamma_N A_{0,\mathrm{ex}} \quad \text{on } \partial\Omega.\end{aligned}$$

Finally, the definition of ϕ_0 gives

$$\gamma_\nu^- U_0 = (A_0 - \nabla\phi_0) \cdot \nu = 0 \quad \text{on } \partial\Omega,$$

whereas

$$\gamma_\nu^+ U_0 = (A_0 - A_{0,\mathrm{ex}} - \nabla\psi) \cdot \nu \quad \text{on } \partial\Omega.$$

Therefore,

$$[\gamma_\nu U_0] = (A_0 - A_{0,\mathrm{ex}} - \nabla\psi) \cdot \nu \quad \text{on } \partial\Omega. \tag{16}$$

Collecting the preceding identities, we conclude that U_0 satisfies the transmission problem

$$\begin{aligned}\operatorname{curl}\operatorname{curl} U_0 &= 0 && \text{in } \mathbb{R}^3 \setminus \overline{\Omega}, \\ \operatorname{curl}\operatorname{curl} U_0 + U_0 &= \mathbf{f}_{\mathrm{ex}} && \text{in } \Omega, \\ [\gamma_\tau U_0] &= -\gamma_\tau A_{0,\mathrm{ex}} && \text{on } \partial\Omega, \\ [\gamma_N U_0] &= -\gamma_N A_{0,\mathrm{ex}} && \text{on } \partial\Omega, \\ [\gamma_\nu U_0] &= \gamma_\nu^+ (A_0 - A_{0,\mathrm{ex}} - \nabla\psi) && \text{on } \partial\Omega, \\ \lim_{|x|\to\infty} |U_0(x)| &= 0. \end{aligned} \tag{17}$$

Although the normal jump (16) does not vanish in general, it will not enter the coupled FEM–BEM formulation developed in Section 5. Indeed, the exterior normal trace appears only through a gradient term in the representation formula for U_0, which vanishes upon application of the curl trace γ_N^+.

Thus, the computation of H_0 reduces to solving the transmission problem (17) for U_0 and subsequently recovering H_0 from (15). Once H_0 has been determined, B_0 is obtained by solving the constrained curl–curl problem (3), with H_0 as its source term.

To obtain a well-posed weak formulation of (3), we use the Kikuchi formulation [Kik87] which relies on the homogeneous boundary conditions spaces given by

$$\begin{aligned}\mathring{H}(\operatorname{curl}, \Omega) &:= \{H \in H(\operatorname{curl}, \Omega) : H \times \nu = 0 \text{ on } \partial\Omega\}, \\ \mathring{H}^1(\Omega) &:= \left\{p \in H^1(\Omega) : p = 0 \text{ on } \partial\Omega\right\},\end{aligned}$$

where we have chosen a circle above the H and not a zero below (the more common choice) to avoid confusion with the variable H_0. The Kikuchi formulation of Maxwell's equations thus reads: Find $B_0 \in \mathring{H}(\operatorname{curl}, \Omega)$ and $p \in \mathring{H}^1(\Omega)$ such that

$$\begin{aligned}(\operatorname{curl} B_0, \operatorname{curl} B^*) + (\nabla p, B^*) &= (H_0, B^*) && \forall B^* \in \mathring{H}(\operatorname{curl}, \Omega), \\ (\nabla p^*, B_0) &= 0 && \forall p^* \in \mathring{H}^1(\Omega).\end{aligned} \tag{18}$$

This problem is equivalent to (3). Its well-posedness follows from [BBF13, Theorem 11.2.1].

Proposition 4.1 ([BBF13, Theorem 11.2.1])**.** *The bilinear form* $b\colon \mathring{H}(\mathrm{curl},\Omega)\times\mathring{H}^1(\Omega)\to\mathbb{R}$, *defined by* $b(B,p)\coloneqq(\nabla p, B)$, *satisfies the inf-sup condition*

$$\inf_{p\in\mathring{H}^1(\Omega)\setminus\{0\}}\ \sup_{B\in\mathring{H}(\mathrm{curl},\Omega)\setminus\{0\}} \frac{b(B,p)}{\|B\|_{H(\mathrm{curl},\Omega)}\|p\|_{H^1(\Omega)}}\geq\beta>0.$$

Proof. For any $p\in\mathring{H}^1(\Omega)$, set $B=\nabla p$. Since $p|_{\partial\Omega}=0$, we have $\nabla_{\partial\Omega}p=0$ on $\partial\Omega$, and hence $\nabla p\times\nu=\nabla_{\partial\Omega}p\times\nu=0$, so that $B\in\mathring{H}(\mathrm{curl},\Omega)$. Moreover, $\mathrm{curl}\,\nabla p=0$, and therefore $\|\nabla p\|_{H(\mathrm{curl},\Omega)}=\|\nabla p\|_{L^2(\Omega)}$. Then

$$\sup_{B\in\mathring{H}(\mathrm{curl},\Omega)}\frac{b(B,p)}{\|B\|_{H(\mathrm{curl},\Omega)}}\geq\frac{b(\nabla p,\,p)}{\|\nabla p\|_{H(\mathrm{curl},\Omega)}}=\|\nabla p\|_{L^2(\Omega)}\geq c\|p\|_{H^1(\Omega)},$$

where the last inequality follows from Poincaré's inequality. $\square$

Furthermore, the bilinear form $a(B,B^*)\coloneqq(\mathrm{curl}\,B,\mathrm{curl}\,B^*)$ is coercive on $\{B\in\mathring{H}(\mathrm{curl},\Omega): \mathrm{div}\,B=0\}$. Indeed, [Mon03, Corollary 4.8] gives

$$\|B\|_{L^2(\Omega)}\leq C\|\mathrm{curl}\,B\|_{L^2(\Omega)}$$

for all B in this space, so that

$$a(B,B)=\|\mathrm{curl}\,B\|^2_{L^2(\Omega)}\geq\frac{1}{1+C^2}\|B\|^2_{H(\mathrm{curl},\Omega)}.$$

The well-posedness of (18) then follows from the Babuška–Brezzi theory [BBF13, Theorem 11.2.1].

5. Numerical Approximation of the London Equation

In this section, we provide a numerical framework that yields a provably convergent approximation of the magnetic field H_0 and the vector field B_0. We formulate Galerkin schemes for (17) and (18). The FE approximation of the solutions will be computed on a regular family of tetrahedral meshes $\mathcal{T}_h$ of Ω, indexed by the mesh size h, satisfying $\Omega_h=\bigcup_{K\in\mathcal{T}_h}K$. The induced triangulation on $\partial\Omega_h$, consisting of the triangular faces of elements in $\mathcal{T}_h$ lying on the boundary, is denoted $\mathcal{F}_h$.

Given a polynomial degree $k\geq1$, on $\mathcal{T}_h$ we consider the Lagrange space [Mon03, Section 5.2]

$$\mathbb{P}_k(\mathcal{T}_h)\subset H^1(\Omega)$$

of continuous piecewise polynomials of degree k, and the Nédélec space [Mon03, Section 5.5]

$$\mathrm{NED}_k(\mathcal{T}_h)\subset H(\mathrm{curl},\Omega)$$

of $H(\mathrm{curl})$ conforming elements with tangential continuity. On the surface mesh $\mathcal{F}_h$, we consider the Rao–Wilton–Glisson space

$$\mathrm{RWG}(\mathcal{F}_h)\subset H^{-1/2}(\mathrm{div}_{\partial\Omega},\partial\Omega).$$

We further introduce a dual barycentric mesh $\widetilde{\mathcal{F}}_h$ of $\partial\Omega_h$, on which we define the Buffa–Christiansen space [BC07]

$$\mathrm{BC}(\widetilde{\mathcal{F}}_h)\subset H^{-1/2}(\mathrm{div}_{\partial\Omega},\partial\Omega),$$

which serves as the test space in the stable duality pairing $\langle\cdot,\cdot\rangle_\times$ between $H^{-1/2}(\mathrm{div}_{\partial\Omega},\partial\Omega)$ and itself.

5.1. **Approximation of the magnetic field H_0.** In order to discretize (17) and solve for H_0, we aim to find $U_0 \in H(\mathrm{curl}, \mathbb{R}^3 \setminus \partial\Omega)$ satisfying the interior variational equation

$$(\mathrm{curl}\, U_0, \mathrm{curl}\, U_0^*) + (U_0, U_0^*) - \langle \gamma_N^- U_0, \gamma_\tau^- U_0^* \rangle_{\partial\Omega} = (\mathbf{f}_{\mathrm{ex}}, U_0^*) \quad \forall U_0^* \in H(\mathrm{curl}, \Omega),$$

and the jump conditions of (17)

$$\begin{aligned} [\gamma_\tau U_0] &= -\gamma_\tau A_{0,\mathrm{ex}} && \text{on } \partial\Omega, \\ [\gamma_N U_0] &= -\gamma_N A_{0,\mathrm{ex}} && \text{on } \partial\Omega, \\ [\gamma_\nu U_0] &= \gamma_\nu^+ (A_0 - A_{0,\mathrm{ex}} - \nabla\psi) && \text{on } \partial\Omega. \end{aligned} \tag{19}$$

For the exterior problem, we use a representation of U_0 in $\mathbb{R}^3 \setminus \overline{\Omega}$ based on integral operators and the fundamental solution of the Laplace problem (see Proposition B.4 in Appendix B). The representation is given by

$$U_0(x) = \mathbf{\Psi}_{\mathrm{DL}}(\gamma_\tau^+ U_0)(x) - \mathbf{\Psi}_{\mathrm{SL}}(\gamma_N^+ U_0)(x) + \nabla \Psi_{\mathrm{SL}}(\gamma_\nu^+ U_0)(x), \qquad \text{for } x \in \mathbb{R}^3 \setminus \overline{\Omega}. \tag{20}$$

Note that in (20) we explicitly observe that a non vanishing exterior normal trace of U_0 appears as a gradient contribution in the exterior field. We can obtain boundary integral equations for $\gamma_\tau^+ U_0$ and $\gamma_N^+ U_0$ by applying trace operators to (20). Since the curl of a gradient is always zero, by applying γ_N^+ to (20), we obtain

$$-\mathbf{W}_0(\gamma_\tau^+ U_0) + \left(\tfrac{1}{2}\mathbf{I} + \mathbf{K}_0\right)(\gamma_N^+ U_0) = 0, \tag{21}$$

where we used boundary integral operators as defined in (27) in Appendix B. It becomes clear that we only need information on tangential traces to solve our problem of interest. These are bounded operators from $H^{-1/2}(\mathrm{div}_{\partial\Omega}, \partial\Omega)$ to itself. Using (21), we can define a continuous version of a Steklov–Poincaré operator.

The duality pairing that makes $H^{-1/2}(\mathrm{div}_{\partial\Omega}, \partial\Omega)$ its own dual involves a rotation: for $\lambda, \lambda^* \in H^{-1/2}(\mathrm{div}_{\partial\Omega}, \partial\Omega)$, we define

$$\langle \lambda, \lambda^* \rangle_\times \coloneqq \langle \lambda, \nu \times \lambda^* \rangle.$$

We denote $\eta \coloneqq \gamma_\tau^- U_0$ and $\lambda \coloneqq \gamma_N^- U_0$. Then (21) combined with the jump conditions (19) leads to

$$-\mathbf{W}_0 \eta + \left(\tfrac{1}{2}\mathbf{I} + \mathbf{K}_0\right)\lambda = \mathbf{W}_0(\gamma_\tau A_{0,\mathrm{ex}}) - \left(\tfrac{1}{2}\mathbf{I} + \mathbf{K}_0\right)(\gamma_N A_{0,\mathrm{ex}}) =: \lambda_{0,\mathrm{ex}}.$$

A weak formulation for (21) reads as follows: we seek $\lambda \in H^{-1/2}(\mathrm{div}_{\partial\Omega} 0, \partial\Omega)$ such that

$$-\langle \mathbf{W}_0 \eta, \lambda^* \rangle_\times + \langle \left(\tfrac{1}{2}\mathbf{I} + \mathbf{K}_0\right)\lambda, \lambda^* \rangle_\times = \langle \lambda_{0,\mathrm{ex}}, \lambda^* \rangle_\times \qquad \forall \lambda^* \in H^{-1/2}(\mathrm{div}_{\partial\Omega} 0, \partial\Omega),$$

where $H^{-1/2}(\mathrm{div}_{\partial\Omega} 0, \partial\Omega)$ is defined in Appendix B, eq. (29).

Lemma 5.1. *The operator $\mathbf{K}_0 : H^{-1/2}(\mathrm{div}_{\partial\Omega}, \partial\Omega) \to H^{-1/2}(\mathrm{div}_{\partial\Omega}, \partial\Omega)$ is compact.*

We are interested in the coupling: find $(U, \lambda) \in H(\mathrm{curl}, \Omega) \times H^{-1/2}(\mathrm{div}_{\partial\Omega} 0, \partial\Omega)$ such that

$$\begin{aligned} (\mathrm{curl}\, U_0, \mathrm{curl}\, U_0^*) + (U_0, U_0^*) - \langle \lambda, \gamma_\tau^- U_0^* \rangle_\times &= (\mathbf{f}_{\mathrm{ex}}, U_0^*) && \forall U_0^* \in H(\mathrm{curl}, \Omega), \\ -\langle \mathbf{W}_0 \gamma_\tau^- U_0, \lambda^* \rangle_\times + \langle \left(\tfrac{1}{2}\mathbf{I} + \mathbf{K}_0\right)\lambda, \lambda^* \rangle_\times &= \langle \lambda_{0,\mathrm{ex}}, \lambda^* \rangle && \forall \lambda^* \in H^{-1/2}(\mathrm{div}_{\partial\Omega}, \partial\Omega). \end{aligned} \tag{22}$$

Definition 5.1 (Steklov–Poincaré operator)**.** *The operator*

$$\mathbf{S}_0 \colon H^{-1/2}(\mathrm{div}_{\partial\Omega}, \partial\Omega) \to H^{-1/2}(\mathrm{div}_{\partial\Omega} 0, \partial\Omega)$$

is defined by

$$\mathbf{S}_0 \eta \coloneqq \left(\tfrac{1}{2}\mathbf{I} + \mathbf{K}_0\right)^{-1} \mathbf{W}_0\, \eta, \qquad \eta \in H^{-1/2}(\mathrm{div}_{\partial\Omega}, \partial\Omega),$$

equivalently characterized, for $\eta \in H^{-1/2}(\mathrm{div}_{\partial\Omega}, \partial\Omega)$*, as the unique* $\mu := \mathbf{S}_0\eta$ *satisfying*

$$\left\langle (\tfrac{1}{2}\mathbf{I} + \mathbf{K}_0)\mu,\ \mu^* \right\rangle_\times = \langle \mathbf{W}_0\eta,\ \mu^*\rangle_\times \qquad \forall\, \mu^* \in H^{-1/2}(\mathrm{div}_{\partial\Omega}\, 0, \partial\Omega).$$

The reduced, one-field bilinear form $q\colon H(\mathrm{curl}, \Omega) \times H(\mathrm{curl}, \Omega) \to \mathbb{R}$ associated with (22) is defined by

$$q(U_0, U_0^*) := (\mathrm{curl}\, U_0, \mathrm{curl}\, U_0^*) + (U_0, U_0^*) - \left\langle \mathbf{S}_0\, \gamma_\tau^- U_0,\ \gamma_\tau^- U_0^* \right\rangle_\times, \qquad U_0, U_0^* \in H(\mathrm{curl}, \Omega).$$

Proposition 5.2 (Inf-sup condition for the reduced coupling)**.** *Let* $\Omega \subset \mathbb{R}^3$ *be a bounded domain with smooth connected boundary* $\partial\Omega$*. The bilinear form* q *satisfies the inf-sup condition*

$$\inf_{\substack{U_0 \in H(\mathrm{curl},\Omega) \\ U_0 \neq 0}} \ \sup_{\substack{U_0^* \in H(\mathrm{curl},\Omega) \\ U_0^* \neq 0}} \frac{q(U_0, U_0^*)}{\|U_0\|_{H(\mathrm{curl},\Omega)}\, \|U_0^*\|_{H(\mathrm{curl},\Omega)}} \ \geq\ \beta\ >\ 0.$$

Proof. Since $\mathbf{K}_0$ is a compact operator from $H^{-1/2}(\mathrm{div}_{\partial\Omega}, \partial\Omega)$ to itself, the operator $\mathbf{S}_0$ has a principal part corresponding to $2\mathbf{W}_0$. Then, it is enough to show that the bilinear form

$$q_0(U_0, U_0^*) := (\mathrm{curl}\, U_0, \mathrm{curl}\, U_0^*) + (U_0, U_0^*) - \left\langle 2\mathbf{W}_0\, \gamma_\tau^- U_0,\ \gamma_\tau^- U_0^* \right\rangle_\times, \qquad U_0, U_0^* \in H(\mathrm{curl}, \Omega).$$

satisfies an inf-sup condition with a constant β_0. Choose a test function $U_0^* = U_0 + V_0 \in H(\mathrm{curl}, \Omega)$. Let V_0 be the solution of

$$(\mathrm{curl}\, V_0, V_0^*) + (V_0, V_0^*) = \langle 2\mathbf{W}_0\gamma_\tau^- U_0, V_0^*\rangle_\times \qquad \forall V_0^* \in H(\mathrm{curl}, \Omega). \tag{23}$$

Then, from (23), we can rewrite

$$\begin{aligned} q_0(U_0, U_0 + V_0) &= \|U_0\|^2_{H(\mathrm{curl},\Omega)} + (\mathrm{curl}\, U_0, \mathrm{curl}\, V_0) + (U_0, V_0) \\ &\quad - \left\langle 2\mathbf{W}_0\, \gamma_\tau^- U_0,\ \gamma_\tau^- U_0 \right\rangle_\times - \left\langle 2\mathbf{W}_0\, \gamma_\tau^- U_0,\ \gamma_\tau^- V_0 \right\rangle_\times \end{aligned}$$

into

$$q_0(U_0, U_0 + V_0) = \|U_0\|^2_{H(\mathrm{curl},\Omega)} - \|V_0\|^2_{H(\mathrm{curl},\Omega)}.$$

Hence, it remains to show that $\|V_0\|_{H(\mathrm{curl},\Omega)} \leq c\|U_0\|_{H(\mathrm{curl},\Omega)} < \|U_0\|_{H(\mathrm{curl},\Omega)}$ for some $c \in (0, 1)$, which follows from a standard contraction argument involving the operator $\mathbf{K}_0$; see [EEK21, Ste11]. $\square$

In order to have a stable discrete duality pairing $\langle\cdot,\cdot\rangle_\times$ in $H^{-1/2}(\mathrm{div}_{\partial\Omega}, \partial\Omega)$, we rely on the pairing of $\mathrm{RWG}(\mathcal{F}_h)$ (for trial) and $\mathrm{BC}(\widetilde{\mathcal{F}}_h)$ (for test) boundary element spaces. Therefore, we solve for $(U_{0,h}, \lambda_h) \in \mathrm{NED}(\mathcal{T}_h) \times \mathrm{RWG}(\mathcal{F}_h)$ such that

$$\begin{aligned} (\mathrm{curl}\, U_{0,h}, \mathrm{curl}\, U_{0,h}^*) + (U_{0,h}, U_{0,h}^*) - \langle \lambda_h, \gamma_\tau^- U_{0,h}^*\rangle_\times &= (\mathbf{f}_{\mathrm{ex}}, U_{0,h}^*) \quad \forall U_{0,h}^* \in \mathrm{NED}_k(\mathcal{T}_h), \\ -\langle \mathbf{W}_0\gamma_\tau^- U_{0,h}, \lambda_h^*\rangle_\times + \langle \left(\tfrac{1}{2}\mathbf{I} + \mathbf{K}_0\right) \lambda_h, \lambda_h^*\rangle_\times &= \langle \lambda_{\mathrm{ex}}, \lambda_h^*\rangle \quad \forall \lambda_h^* \in \mathrm{BC}(\widetilde{\mathcal{F}}_h). \end{aligned}$$

5.2. **Approximation of the vector field B_0.** Consider the conforming FE spaces

$$\begin{aligned} V_h^B &:= \mathrm{NED}_k(\mathcal{T}_h) \cap \mathring{H}(\mathrm{curl}, \Omega), \\ V_h^p &:= \mathbb{P}_k(\mathcal{T}_h) \cap \mathring{H}^1(\Omega). \end{aligned}$$

The discrete Galerkin formulation then looks for $(B_{0,h}, p_h)$ in $V_h^B \times V_h^p$ such that

$$\begin{aligned} (\mathrm{curl}\, B_{0,h}, \mathrm{curl}\, B_{0,h}^*) + (\nabla\, p_h, B_{0,h}^*) &= \langle H_0, B_{0,h}^*\rangle \quad \forall B_{0,h}^* \in V_h^B, \\ (\nabla\, p_h^*, B_{0,h}) &= 0 \qquad\qquad\quad \forall p_h^* \in V_h^p. \end{aligned} \tag{24}$$

Lemma 5.3. *Problem* (24) *is well-posed.*

Proof. This result is shown in [BBF13, Theorem 11.2.2] and its proof relies on the Babuška–Brezzi theory. Indeed, the discrete spaces have been chosen such that $\nabla V_h^p \subset V_h^B$, which immediately yields the discrete inf-sup stability of the bilinear form $(\nabla p_h^*, B_{0,h})$. Ellipticity of the positive part $(\operatorname{curl} B_{0,h}, \operatorname{curl} B_{0,h}^*)$ is a consequence of the discrete Friedrichs inequality. □

The Ladysenskaya–Babuška–Brezzi theory establishes the convergence of the proposed FE scheme for (24), which yields the following result:

Theorem 1. *If B_0 belongs to $H^s(\operatorname{curl}, \Omega)$ with $1/2 < s \leq k$, then the solutions $B_{0,h}$ and B_0 satisfy the following error estimate:*

$$\|B_0 - B_{0,h}\|_{H_0(\operatorname{curl},\Omega)} \leq C\|B_0\|_{H^s(\operatorname{curl},\Omega)} h^s,$$

for some generic mesh-independent constant C.

Proof. This is a standard consequence of the Ceá estimate satisfied by the solution of (24) as in [BBF13, Corollary 11.2.1] and the convergence properties of the Nédélec interpolator [Mon03, Theorem 5.41]. □

5.3. **Convergence of the overall formulation.** Given that each sub-problem ((17) and (18)) enjoys standard optimal convergence rates (under sufficient regularity), the final concern regards the convergence of the entire procedure, i.e. the computations

(1) of the magnetic field $H_{0,h}$,
(2) and of the vector field $B_{0,h} \coloneqq B_{0,h}(H_{0,h})$.

We now proceed to derive a Strang estimate, which directly establishes the results we are looking for.

5.4. **Strang estimate for $B_{0,h}$.** We modify the formulation of (24) to have a mesh-dependent right hand side by replacing H_0 with $H_{0,h}$. Then, the errors $e_h^B \coloneqq B_0 - B_{0,h}$, $e_h^H \coloneqq H_0 - H_{0,h}$, and $e_h^p \coloneqq p - p_h$ satisfy the equation

$$\begin{aligned} (\operatorname{curl} e_h^B, \operatorname{curl} B_{0,h}^*) + (\nabla e_h^p, B_{0,h}^*) &= (\operatorname{curl} e_h^H, \operatorname{curl} B_{0,h}^*) \quad && \forall B_{0,h}^* \in V_h^B \\ (\nabla p_h^*, e_h^B) &= 0 && \forall p_h^* \in V_h^p. \end{aligned} \tag{25}$$

This yields the following convergence result.

Lemma 5.4. *If the error in the magnetic field converges as $\|e_h^H\|_{\operatorname{curl}} \leq Ch^k$, then the following convergence estimate holds:*

$$\|B_0 - B_{0,h}\|_{\operatorname{curl}} \leq Ch^k.$$

Proof. Consider e_h^B the solution to (25), which is guaranteed to exist in virtue of Lemma 5.3. Then, the discrete Friedrich inequality yields the existence of some constant $c > 0$ such that

$$c\|e_h^B\|_{\operatorname{curl}} \leq \|\operatorname{curl} e_h^B\|_{L^2}.$$

This, together with the previously used fact that $p_h = p = 0$ [BBF13] yields that

$$c^2\|e_h^B\|_{\operatorname{curl}}^2 \leq \|\operatorname{curl} e_h^B\|_{L^2}^2 \leq (\operatorname{curl} e_h^H, \operatorname{curl} e_h^B) \leq \|e_h^H\|_{\operatorname{curl}}\|e_h^B\|_{\operatorname{curl}},$$

which establishes the desired result. □

6. Numerical tests

In this section we propose numerical tests to validate our convergence theory. These tests are:

(1) Validation of the convergence rates computed in Section 5 for the variables $H_{0,h}$ and $B_{0,h}$ using a manufactured-solution approach.
(2) Theoretical validation test, in which we solve for B_0 on a ball and compare the numerical solution to the analytical one available in Appendix A.

6.1. **Numerical convergence.**

6.1.1. *U_0 problem.* In this section, we validate the convergence of problem (22) using a manufactured-solution approach. For this, we consider an analytic solution, given by

$$U_0(x,y,z) = \begin{bmatrix} e^x \sin(y) \\ e^x \cos(y) \\ 0 \end{bmatrix},$$

in Ω and zero in the exterior. We compensate the right hand side accordingly for this study in Ω. The results are reported in Table 1, where the convergence rates expected from the theory are observed. The definitions used are given by

$$e_U^h := \|U_0 - U_{0,h}\|_{H(\mathrm{curl},\Omega)}, \qquad r_U := \frac{\log \frac{e_U^h}{e_U^{h'}}}{\log \frac{h}{h'}}.$$

DoFs	e_U^h	r_U
1043	1.66e-01	–
1345	1.46e-01	1.13
3764	1.05e-01	0.91
25362	5.54e-02	0.98
48409	4.48e-02	1.08
111917	3.33e-02	0.96
187186	2.80e-02	1.02

Table 1. Convergence test: Manufactured solutions for U_0.

6.1.2. *B_0 problem.* In this section, we provide a manufactured solution to problem (24) and study the convergence with respect to it. The analytical solution we consider is

$$B(x,y) = \begin{bmatrix} x^2y - y^2 \\ x^2 - xy^2 \end{bmatrix},$$

which we impose on the entire boundary as a Dirichlet boundary condition. Note that the analytical pressure is $p = 0$. We perform this for a uniform refinement of the mesh and obtain the optimal rates reported in Table 2, as expected from the theory. The discrete pressure is zero up to machine precision. Note that, in the table, we have used the following definitions:

$$e_B^h := \|B - B_h\|_{H(\mathrm{curl},\Omega)}, \qquad e_p^h := \|p_h\|_{H^1(\Omega)},$$

$$r_B := \frac{\log \frac{e_B^h}{e_B^{h'}}}{\log \frac{h}{h'}}, \qquad r_p := \frac{\log \frac{e_p^h}{e_p^{h'}}}{\log \frac{h}{h'}}.$$

DoFs	e_B^h	r_B	e_p^h	r_p
25	3.00e-01	–	3.09e-16	–
81	1.73e-01	0.80	1.11e-14	-5.17
289	9.33e-02	0.89	1.17e-14	-0.07
1089	4.85e-02	0.94	3.02e-13	-4.69
4225	2.48e-02	0.97	4.07e-12	-3.75
16641	1.25e-02	0.99	4.45e-11	-3.45

TABLE 2. Convergence test: Manufactured solutions for B_0.

6.2. **Theoretical validation with an analytic solution.** In this section, we study the convergence of the solution in a curved domain, namely the unit ball, against a well-known analytic solution for $H_{0,\mathrm{ex}} = (0,0,1)$, with $A_{0,\mathrm{ex}}(x,y,z) = \frac{1}{2}(y,-x,0)$. The full expression is provided in Appendix A, and we provide the convergence for the problem's variables in Table 3. Note that in the table, we have used the following definitions:

$$e_{B_0}^h := \|B_0 - B_{0,h}\|_{H(\mathrm{curl},\Omega)}, \qquad e_{U_0}^h := \|U_0 - U_{0,h}\|_{H(\mathrm{curl},\Omega)},$$

$$r_{B_0} := \frac{\log \frac{e_{B_0}^h}{e_{B_0}^{h'}}}{\log \frac{h}{h'}}, \qquad r_{U_0} := \frac{\log \frac{e_{U_0}^h}{e_{U_0}^{h'}}}{\log \frac{h}{h'}}.$$

DoFs	$e_{U_0}^h$	r_{U_0}	$e_{B_0}^h$	r_{B_0}
1043	2.45e-02	–	1.79e-01	–
1345	2.12e-02	1.24	1.59e-01	1.04
3764	1.49e-02	0.98	1.10e-01	1.02
25362	7.21e-03	1.11	5.51e-02	1.06
48409	5.74e-03	1.16	4.39e-02	1.15
111917	4.27e-03	0.96	3.28e-02	0.94
187186	3.56e-03	1.06	2.74e-02	1.04

TABLE 3. Convergence test: Analytic solution for U_0 and B_0.

The recovered rates are as expected from the theory. We further show the discrete solution $B_{0,h}$ and the discrete approximation of $H_{0,h}$, given by $\mathrm{curl}\, U_{0,h}$, in Figure 2. Note that there are some oscillations present in $H_{0,h}$, mainly towards the boundary, as it is the discrete gradient of a FE field.

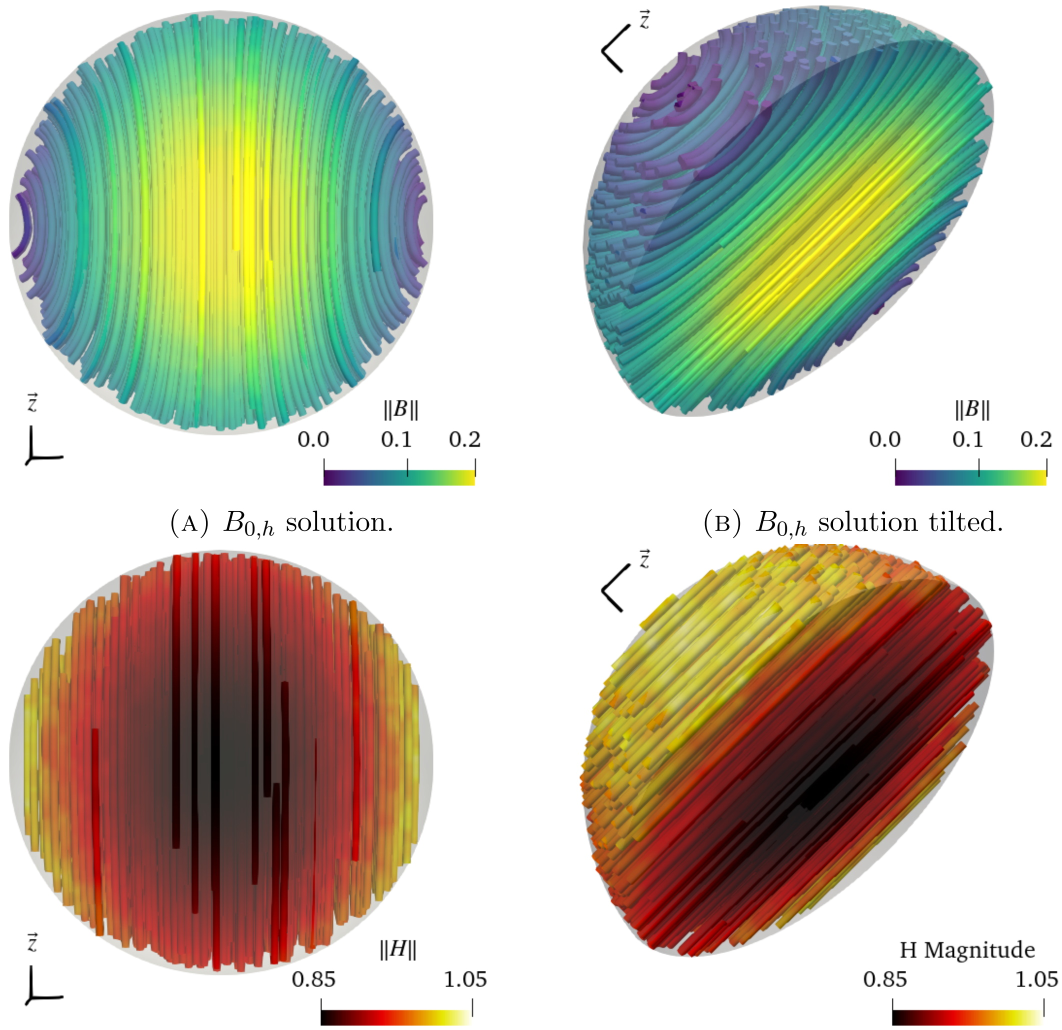

(A) $B_{0,h}$ solution.

(B) $B_{0,h}$ solution tilted.

(C) $H_{0,h}$ solution.

(D) $H_{0,h}$ solution tilted.

FIGURE 2. Theoretical validation test on the unit ball.

7. Application to the isoflux problem

We consider the prolate ellipsoid

$$\Omega = \left\{ (x, y, z) \in \mathbb{R}^3 : \frac{x^2 + y^2}{a^2} + z^2 < 1 \right\}, \qquad 0 < a < 1,$$

and assume that the normalized applied magnetic field is

$$H_{0,\text{ex}} = \hat{z}.$$

Thus, the major axis of the ellipsoid is aligned with the z-direction, while the two minor semi-axes, in the x- and y-directions, have length a. Since both the domain and the direction of the applied field are invariant under rotations around the major axis, the corresponding field B_0 is independent of the azimuthal angle and has no component in the azimuthal direction. As in the analysis of the isoflux problem for the ball carried out in [ABM06, Rom19], this axisymmetry naturally reduces the problem to curves contained in two-dimensional sections determined by planes containing the major axis and lying entirely on one side of this axis. We work in the section determined by the (x,z)-plane and, without loss of generality, consider curves lying on the side $x \geq 0$ of the major axis. The boundary of this section is the ellipse

$$\frac{x^2}{a^2} + z^2 = 1.$$

Let Γ be an oriented curve contained in this section, lying entirely on one side of the major axis and with endpoints on the boundary of the ellipse. As illustrated in Figure 3, we denote by Γ_{bd} the portion of the boundary of the ellipse joining the endpoints of Γ, oriented so that $\Gamma \cup \Gamma_{\mathrm{bd}}$ forms a closed curve. We then denote by S_Γ the region enclosed by this curve. In particular,

$$\Gamma_{\mathrm{bd}} = \partial S_\Gamma \cap \partial\Omega.$$

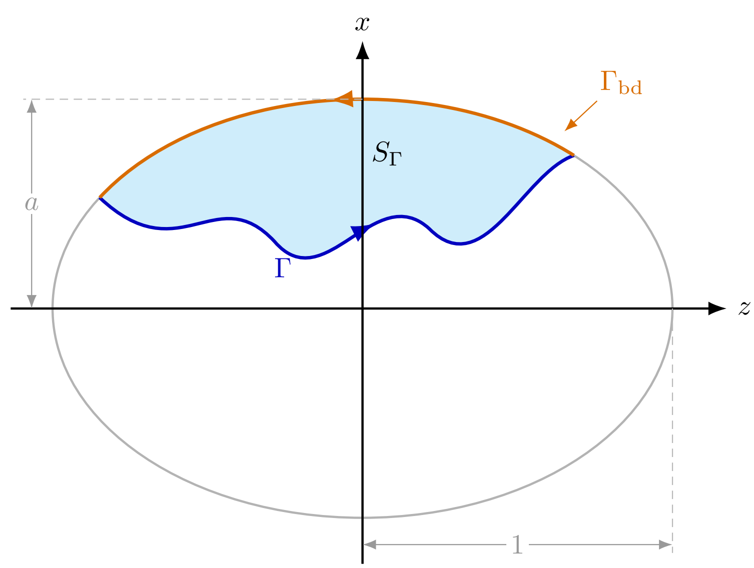

FIGURE 3. An oriented curve Γ lying on one side of the major axis and the region S_Γ enclosed by Γ and the corresponding boundary curve Γ_{bd}.

The boundary condition $B_0 \times \nu = 0$ on $\partial\Omega$ is crucial here, since it implies that B_0 has no tangential component along Γ_{bd} and hence

$$\int_{\Gamma_{\mathrm{bd}}} B_0 \cdot d\ell = 0.$$

We may therefore close Γ along the boundary without changing its line integral:

$$\int_\Gamma B_0 \cdot d\ell = \int_{\partial S_\Gamma} B_0 \cdot d\ell.$$

Applying Stokes' theorem in the oriented (x,z)-section yields

$$\int_\Gamma B_0 \cdot d\ell = \int_{S_\Gamma} \operatorname{curl} B_0 \cdot \hat{y}\, dS,$$

where $\hat{y}$ is the oriented unit normal to the section. The flux density $\operatorname{curl} B_0 \cdot \hat{y}$ is nonnegative; see [RSS23, Section 3].

Consequently, the argument used for the ball in [ABM06, Rom19] also applies in the present setting and shows that a curve whose length exceeds that of the major axis cannot be optimal, since its isoflux ratio is smaller than the one attained by the major axis. Moreover, this analysis allows us to restrict our numerical study to curves that are symmetric with respect to the x-axis, meet the boundary of the ellipse orthogonally, and have an associated region S_Γ that is convex.

Motivated by these geometric properties, we introduce a two-parameter family of piecewise-linear competitors $\Gamma_{(x_0,\lambda)}$. The construction is illustrated in Figure 4 and described in detail next. The parameter x_0 determines the endpoints of the curve on the boundary of the ellipse, while λ controls how far the curve follows the inward normal direction before turning parallel to the major axis.

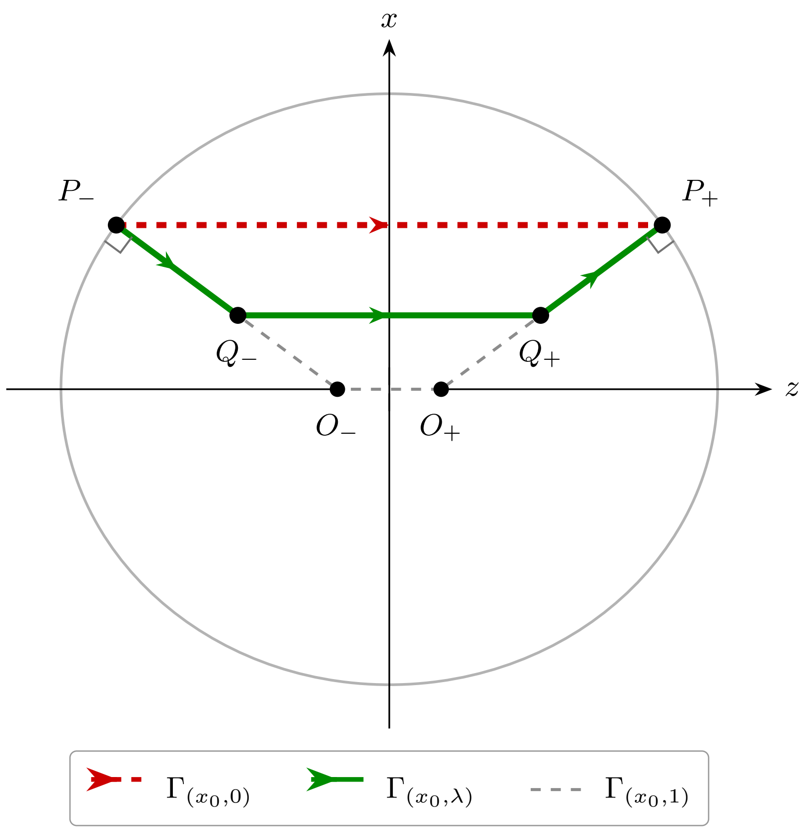

FIGURE 4. Geometric construction of the family $\Gamma_{(x_0,\lambda)}$ in the (x,z)-section of the ellipsoid. The figure shows the limiting configuration $\Gamma_{(x_0,0)}$, an intermediate competitor $\Gamma_{(x_0,\lambda)}$, and the configuration $\Gamma_{(x_0,1)}$, which reaches and follows the major axis.

Fix $x_0 \in (0,a)$ and define

$$z_0 = \sqrt{1-\left(\frac{x_0}{a}\right)^2}, \qquad P_\pm = (x_0, \pm z_0) \in \partial\Omega.$$

For $\lambda \in [0,1]$, set

$$z_\lambda = z_0(1-\lambda a^2), \qquad Q_\pm = \big(x_0(1-\lambda), \pm z_\lambda\big).$$

For $\lambda \in (0,1]$, the points $Q_\pm$ lie in the interior of Ω, and the segments joining $P_\pm$ to $Q_\pm$ follow the inward normal directions to the ellipse at $P_\pm$. When $\lambda = 1$, the points $Q_\pm$ reach the major axis at

$$O_\pm = \big(0, \pm z_0(1-a^2)\big).$$

For $\lambda \in (0,1]$, we define $\Gamma_{(x_0,\lambda)}$ as the piecewise-linear curve connecting, in order,

$$P_-, \qquad Q_-, \qquad Q_+, \qquad P_+.$$

These curves are symmetric with respect to the x-axis and meet the boundary of the ellipse orthogonally at P_- and P_+. We also include the limiting configuration

$$\Gamma_{(x_0,0)} = [P_-, P_+],$$

which is parallel to the major axis. Unlike the curves corresponding to $\lambda \in (0,1]$, this limiting curve does not meet the boundary orthogonally; it is included to illustrate the full geometric interpolation. At the other endpoint,

$$\Gamma_{(x_0,1)} = [P_-, O_-] \cup [O_-, O_+] \cup [O_+, P_+],$$

which reaches and follows the major axis. Intermediate values of λ interpolate between these two configurations.

Using the notation for the isoflux ratio presented in the Introduction, every curve in the family satisfies

$$\mathrm{R}\big(\Gamma_{(x_0,\lambda)}\big) \leq \mathrm{R}_0\,.$$

Although these piecewise-linear curves are not expected to be maximizers themselves, they provide a simple finite-dimensional family of competitors with which to investigate whether the major axis remains optimal.

For comparison with the major axis, we extend the notation by setting

$$\Gamma_{(0,0)} \coloneqq \big\{(0,0,z) \in \mathbb{R}^3 : -1 \leq z \leq 1\big\}\,.$$

Thus, $\Gamma_{(0,0)}$ denotes the major axis of the ellipsoid.

We numerically solve the London equation and subsequently compute $B_{0,h}$. The resulting fields $B_{0,h}$ and $H_{0,h}$ are shown in Figure 5, which seem visually comparable to the corresponding results for the ball shown in Figure 2 and present similar oscillations in the discrete curl $H_{0,h}$ towards the boundary.

We then evaluate

$$\mathrm{R}\big(\Gamma_{(x_0,\lambda)}\big)$$

for a sample of x_0-values in both the unit ball and the ellipsoid with $a = 0.2$. The left panel of Figure 6 shows that, in the ball case, where $O_+ = O_-$ coincides with the origin, none of the curves in the family considered has an isoflux ratio larger than that of the diameter aligned with the applied field, in agreement with its theoretically established optimality. By contrast, the right panel provides clear numerical evidence that the major axis of the elongated ellipsoid is not optimal, as several off-axis competitors attain a larger isoflux ratio.

To identify the best competitor within the family considered for the ellipsoid, we evaluate $\mathrm{R}\big(\Gamma_{(x_0,\lambda)}\big)$ over a uniform 500×500 grid in the parameter space (x_0, λ). The optimized parameters yield

$$\mathrm{R}\big(\Gamma_{(x_0,\lambda)}\big) > \mathrm{R}\big(\Gamma_{(0,0)}\big),$$

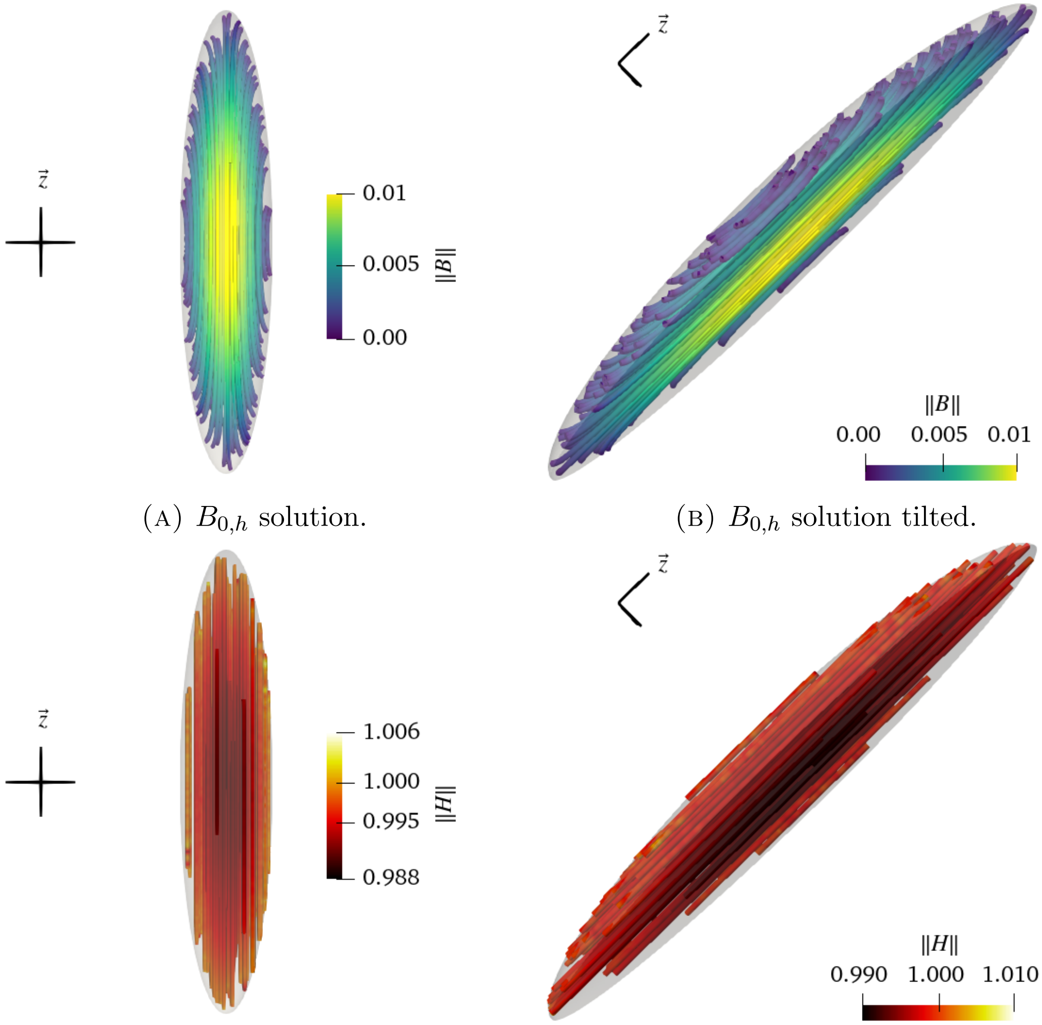

(A) $B_{0,h}$ solution.

(B) $B_{0,h}$ solution tilted.

(C) $H_{0,h}$ solution.

(D) $H_{0,h}$ solution tilted.

FIGURE 5. Discrete fields $H_{0,h}$ and $B_{0,h}$ for the ellipsoid, used to evaluate the isoflux ratio.

providing numerical evidence that the major axis is not optimal when the minor semi-axis is sufficiently small. The corresponding competitor is shown in Figure 7.

Although this comparison does not solve the full isoflux problem in ellipsoids, it provides numerical evidence that the major axis is not a maximizer when a is sufficiently small. The geometry of the best competitors within the family suggests that an isoflux maximizer may instead take the form of a smooth U-shaped configuration, reminiscent of the U-vortices observed experimentally and numerically in rotating Bose–Einstein condensates [RBD02, AD03]; see also [AR01, AJ02, Aft06]. Moreover, rotating any such off-axis configuration around the major axis generates a continuous family of equivalent competitors. This suggests non-uniqueness and the presence of a degenerate rotational direction in the isoflux problem.

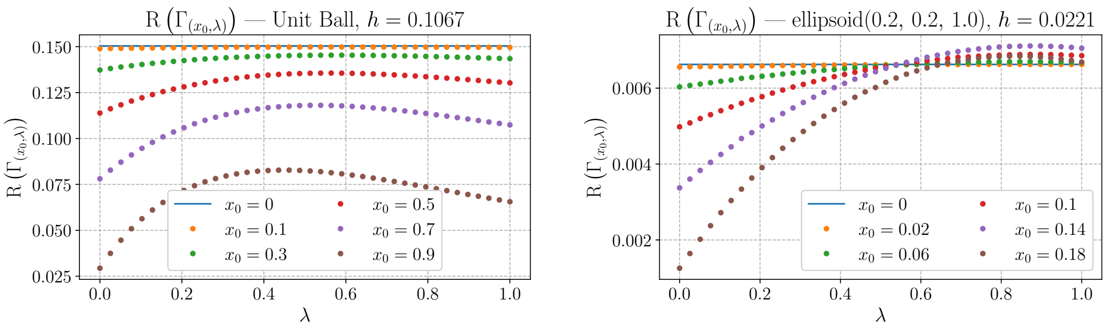

(A) Unit ball. (B) Ellipsoid with $a = 0.2$.

FIGURE 6. Isoflux ratios of the competitors $\Gamma_{(x_0,\lambda)}$ for a sample of x_0-values. For the unit ball (left), none of the competitors considered outperforms the diameter aligned with the applied field. For the elongated ellipsoid (right), some off-axis competitors have a larger isoflux ratio than the major axis.

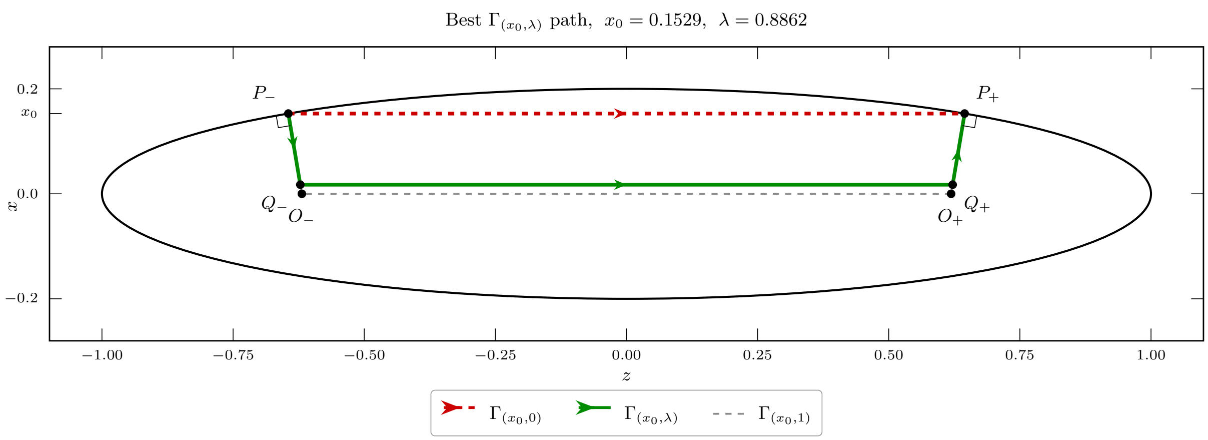

FIGURE 7. Best off-axis competitor within the family considered for the ellipsoid with $a = 0.2$, with an isoflux ratio larger than that of the major axis.

APPENDIX A. EXPLICIT SOLUTION IN A BALL UNDER A UNIFORM NORMALIZED APPLIED FIELD

We recall the explicit solution of the London equation when $\Omega = B(0, R)$ is a ball of radius R centered at the origin and $H_{0,\mathrm{ex}} = \hat{z}$ is the unit vector in the z-direction. This solution will serve as a benchmark for the numerical simulations. Using spherical coordinates (r, θ, ϕ), where r denotes the Euclidean distance from the origin, θ the azimuthal angle, and ϕ the polar angle, we obtain the following explicit formulas; see [Lon50, ABM06].

For $r \geq R$,

$$H_0 = \hat{z} + \frac{2M}{r^3} \cos\phi \hat{r} + \frac{M}{r^3} \sin\phi \hat{\phi} = \left(1 + \frac{2M}{r^3}\right) \cos\phi \hat{r} + \left(-1 + \frac{M}{r^3}\right) \sin\phi \hat{\phi},$$

where

$$M = -\frac{R^3}{2}\left(1 - \frac{3}{R}\coth R + \frac{3}{R^2}\right).$$

For $r \leq R$, the expression becomes

$$H_0 = \frac{3R}{r^2 \sinh R}\left(\cosh r - \frac{\sinh r}{r}\right)\cos\phi\hat{r} + \frac{3R}{2r^2\sinh R}\left(\cosh r - \frac{1+r^2}{r}\sinh r\right)\sin\phi\hat{\phi}.$$

The associated field B_0 is given by

$$B_0 = -\frac{3R}{r^2 \sinh R}\left(\cosh r - \frac{\sinh r}{r}\right)\cos\phi\hat{r} - \frac{3R}{2r^2\sinh R}\left(\cosh r - \frac{1+r^2}{r}\sinh r\right)\sin\phi\hat{\phi} - C\hat{z},$$

where

$$C = \frac{3}{2R\sinh R}\left(\cosh R - \frac{1+R^2}{R}\sinh R\right).$$

Finally, the vector field U_0 defined in (14) is given as follows. For $r \geq R$,

$$U_0 = \frac{M}{r^2}\sin\phi\hat{\theta},$$

where M is the same constant as above. For $r \leq R$,

$$U_0 = \frac{3R}{2\sinh R}\left(\frac{\cosh r}{r} - \frac{\sinh r}{r^2}\right)\sin\phi\hat{\theta}.$$

Appendix B. Boundary integral operators for the exterior problem

This appendix collects the boundary integral operator framework used to handle the exterior equation in (17). That is

$$\begin{aligned} \operatorname{curl}\operatorname{curl} U_0 &= 0 \quad \text{in } \mathbb{R}^3 \setminus \overline{\Omega}, \\ \operatorname{div} U_0 &= 0 \quad \text{in } \mathbb{R}^3 \setminus \overline{\Omega}, \\ \lim_{|x|\to\infty} |U_0(x)| &= 0. \end{aligned} \tag{26}$$

We introduce the fundamental solution, layer potentials, and boundary integral operators. We then establish a representation formula for solutions of the exterior problem (26) that depends only on the boundary data of U_0. This allows us to derive the Calderón equations used in the FEM–BEM coupling.

B.1. **Layer potentials and boundary integral operators.** The fundamental solution of the Laplace equation in $\mathbb{R}^3$ is

$$G_0(x-y) = \frac{1}{4\pi|x-y|}.$$

Using G_0, we define the scalar single-layer potential, the vector single-layer potential, and the vector double-layer potential by

$$\begin{aligned} \Psi_{\mathrm{SL}}(\lambda)(x) &\coloneqq \int_{\partial\Omega} G_0(x-y)\lambda(y)\,\mathrm{d}s_y, && \lambda \in H^{-1/2}(\partial\Omega), \\ \boldsymbol{\Psi}_{\mathrm{SL}}(\mathbf{u})(x) &\coloneqq \int_{\partial\Omega} G_0(x-y)\mathbf{u}(y)\,\mathrm{d}s_y, && \mathbf{u} \in H^{-1/2}(\operatorname{div}_{\partial\Omega}, \partial\Omega), \\ \boldsymbol{\Psi}_{\mathrm{DL}}(\mathbf{u})(x) &\coloneqq \operatorname{curl}\int_{\partial\Omega} G_0(x-y)\mathbf{u}(y)\,\mathrm{d}s_y, && \mathbf{u} \in H^{-1/2}(\operatorname{div}_{\partial\Omega}, \partial\Omega). \end{aligned}$$

From these, we define the boundary integral operators

$$\begin{aligned}\mathbf{V}_0\lambda &:= \tfrac{1}{2}(\gamma_\tau^+ + \gamma_\tau^-)\mathbf{\Psi}_{\mathrm{SL}}\lambda,\\ \mathbf{W}_0\lambda &:= \tfrac{1}{2}(\gamma_N^+ + \gamma_N^-)\mathbf{\Psi}_{\mathrm{DL}}\lambda,\\ \mathbf{K}_0\lambda &:= \tfrac{1}{2}(\gamma_\tau^+ + \gamma_\tau^-)\mathbf{\Psi}_{\mathrm{DL}}\lambda.\end{aligned} \tag{27}$$

These are bounded operators from $H^{-1/2}(\mathrm{div}_{\partial\Omega}, \partial\Omega)$ to itself [BHvPS03]. Moreover, $\mathbf{V}_0$ is elliptic and $\mathbf{K}_0$ is compact on $H^{-1/2}(\mathrm{div}_{\partial\Omega}, \partial\Omega)$; see [BHvPS03].

B.2. **Representation formula.** We begin with two technical lemmas. The first is an identity relating the normal trace of a curl to the surface divergence of the tangential trace.

Lemma B.1. *For $A \in H(\mathrm{curl}, \Omega)$, it holds*

$$\mathrm{curl}\, A \cdot \nu|_{\partial\Omega} = \mathrm{div}_{\partial\Omega}(A \times \nu|_{\partial\Omega}). \tag{28}$$

Lemma B.2. *If $A \in H(\mathrm{curl}, \Omega) \cap H(\mathrm{curl}^2, \Omega)$ with $\mathrm{curl}^2 A = 0$, then*

$$\mathrm{div}_{\partial\Omega}(\mathrm{curl}\, A \times \nu|_{\partial\Omega^-}) = 0.$$

Proof. We use the result of (28) in Lemma B.1 for the vector field $\mathrm{curl}\, A$. It follows that

$$(\mathrm{curl}^2 A) \cdot \nu|_{\partial\Omega} = (\mathrm{curl}(\mathrm{curl}\, A)) \cdot \nu|_{\partial\Omega} = \mathrm{div}_{\partial\Omega}(\mathrm{curl}\, A \times \nu|_{\partial\Omega^-}).$$

Since $\mathrm{curl}^2 A = 0$, we conclude that

$$\mathrm{div}_{\partial\Omega}(\mathrm{curl}\, A \times \nu|_{\partial\Omega^-}) = 0.$$

□

The result of Lemma B.2 illustrates that the natural space for $\mathrm{curl}\, U_0 \times \nu|_{\partial\Omega^+}$, where U_0 satisfies (26), is the subspace of $H^{-1/2}(\mathrm{div}_{\partial\Omega}, \partial\Omega)$ given by

$$H^{-1/2}(\mathrm{div}_{\partial\Omega}\, 0, \partial\Omega) := \left\{\lambda \in H^{-1/2}(\mathrm{div}_{\partial\Omega}, \partial\Omega) : \mathrm{div}_{\partial\Omega}\, \lambda = 0\right\}. \tag{29}$$

The following lemma relates the divergence of the vector single-layer potential to the scalar single-layer potential applied to the surface divergence.

Lemma B.3. *For $\mathbf{u} \in H^{-1/2}(\mathrm{div}_{\partial\Omega}, \partial\Omega)$,*

$$\mathrm{div}\ \mathbf{\Psi}_{\mathrm{SL}}(\mathbf{u}) = \Psi_{\mathrm{SL}}(\mathrm{div}_{\partial\Omega}\, \mathbf{u}).$$

We can now state the representation formula for the exterior problem. Similar results can also be found in [BHvPS03, Hip02b].

Proposition B.4. *Any solution of (26) admits the representation*

$$U_0(x) = \mathbf{\Psi}_{\mathrm{DL}}(\gamma_\tau^+ U_0)(x) - \mathbf{\Psi}_{\mathrm{SL}}(\gamma_N^+ U_0)(x) + \nabla\Psi_{\mathrm{SL}}(\gamma_\nu^+ U_0)(x), \qquad x \in \mathbb{R}^3 \setminus \overline{\Omega}.$$

Conversely, for any $\mathbf{u}, \mathbf{v} \in H^{-1/2}(\mathrm{div}_{\partial\Omega}, \partial\Omega)$ and $\mu \in H^{-1/2}(\partial\Omega)$, the field

$$V(x) := \mathbf{\Psi}_{\mathrm{DL}}(\mathbf{u})(x) - \mathbf{\Psi}_{\mathrm{SL}}(\mathbf{v})(x) + \nabla\Psi_{\mathrm{SL}}(\mu)(x)$$

satisfies $\mathrm{curl}\,\mathrm{curl}\, V = 0$ in $\mathbb{R}^3 \setminus \overline{\Omega}$ and $|V(x)| \to 0$ as $|x| \to \infty$.

Corollary B.1. *The field V defined in Proposition B.4 is additionally divergence-free in $\mathbb{R}^3 \setminus \overline{\Omega}$ if and only if $\mathrm{div}_{\partial\Omega}\, \mathbf{v} = 0$.*

Proof. Since $\boldsymbol{\Psi}_{\mathrm{DL}}(\mathbf{u})$ is the image of a curl operator, we have $\operatorname{div} \boldsymbol{\Psi}_{\mathrm{DL}}(\mathbf{u}) = 0$. Since G_0 is harmonic outside $\partial\Omega$, $\operatorname{div} \nabla \Psi_{\mathrm{SL}}(\mu) = \Delta \Psi_{\mathrm{SL}}(\mu) = 0$. For the remaining term, Lemma B.3 gives $\operatorname{div} \boldsymbol{\Psi}_{\mathrm{SL}}(\mathbf{v}) = \Psi_{\mathrm{SL}}(\operatorname{div}_{\partial\Omega} \mathbf{v})$, which vanishes if and only if $\operatorname{div}_{\partial\Omega} \mathbf{v} = 0$. In particular, taking $\mathbf{v} = \gamma_N^+ U_0$, Lemma B.2 guarantees $\operatorname{div}_{\partial\Omega}(\gamma_N^+ U_0) = 0$ whenever $\operatorname{curl}\operatorname{curl} U_0 = 0$. ☐

B.3. **Calderón equations.** Applying the trace operators γ_τ^+ and γ_N^+ to (20) and using the jump relations for the layer potentials [BHvPS03], one obtains two Calderón equations. Applying γ_τ^+ yields

$$\gamma_\tau^+ U_0 = \left(\tfrac{1}{2}\mathbf{I} + \mathbf{K}_0\right)(\gamma_\tau^+ U_0) - \mathbf{V}_0(\gamma_N^+ U_0) + \mathbf{curl}_{\partial\Omega} \Psi_{\mathrm{SL}}(\gamma_\nu^+ U_0),$$

which rearranges to

$$\left(\tfrac{1}{2}\mathbf{I} - \mathbf{K}_0\right)(\gamma_\tau^+ U_0) + \mathbf{V}_0(\gamma_N^+ U_0) - \mathbf{curl}_{\partial\Omega} \Psi_{\mathrm{SL}}(\gamma_\nu^+ U_0) = 0.$$

Applying γ_N^+ yields

$$\gamma_N^+ U_0 = \mathbf{W}_0(\gamma_\tau^+ U_0) + \left(\tfrac{1}{2}\mathbf{I} - \mathbf{K}_0\right)(\gamma_N^+ U_0),$$

which rearranges to

$$-\mathbf{W}_0(\gamma_\tau^+ U_0) + \left(\tfrac{1}{2}\mathbf{I} + \mathbf{K}_0\right)(\gamma_N^+ U_0) = 0. \tag{30}$$

Equation (30) is a second-kind boundary integral equation for $\gamma_N^+ U_0$, since $\mathbf{K}_0$ is compact [BHvPS03]. This is the one we use in the FEM–BEM coupling; see Section 5.

Acknowledgments

N.B was supported by Centro de Modelamiento Matemático (CMM), Proyecto Basal FB210005. C.R. was supported by ANID FONDECYT 1231593.

References

[ABH+15] M. S. Alnæs, J. Blechta, J. Hake, A. Johansson, B. Kehlet, A. Logg, C. N. Richardson, J. Ring, M. E. Rognes, and G. N. Wells, *The FEniCS project version 1.5*, Arch. Numer. Softw. **3** (2015), no. 100, 9–23. ↑5

[ABM06] S. Alama, L. Bronsard, and J. A. Montero, *On the Ginzburg-Landau model of a superconducting ball in a uniform field*, Ann. Inst. H. Poincaré Anal. Non Linéaire **23** (2006), no. 2, 237–267. MR2201153 ↑4, 17, 18, 22

[AD03] A. Aftalion and I. Danaila, *Three-dimensional vortex configurations in a rotating Bose-Einstein condensate*, Phys. Rev. A **68** (2003), no. 2, 023603. ↑6, 21

[Aft06] A. Aftalion, *Vortices in Bose-Einstein condensates*, Progress in Nonlinear Differential Equations and their Applications, vol. 67, Birkhäuser Boston, Inc., Boston, MA, 2006. ↑21

[AJ02] A. Aftalion and R. L. Jerrard, *Shape of vortices for a rotating Bose-Einstein condensate*, Phys. Rev. A **66** (2002), no. 2, 023611. ↑21

[AR01] A. Aftalion and T. Rivière, *Vortex energy and vortex bending for a rotating Bose-Einstein condensate*, Phys. Rev. A **64** (2001), no. 4, 043611. ↑21

[Arn18] D. N. Arnold, *Finite element exterior calculus*, CBMS-NSF Regional Conference Series in Applied Mathematics, vol. 93, Society for Industrial and Applied Mathematics (SIAM), Philadelphia, PA, 2018. MR3908678 ↑5

[BBF13] D. Boffi, F. Brezzi, and M. Fortin, *Mixed finite element methods and applications*, Springer Series in Computational Mathematics, vol. 44, Springer, Heidelberg, 2013. MR3097958 ↑10, 11, 14

[BC07] A. Buffa and S. H. Christiansen, *A dual finite element complex on the barycentric refinement*, Math. Comp. **76** (2007), no. 260, 1743–1769. MR2336266 ↑5, 11

[BCS02] A. Buffa, M. Costabel, and D. Sheen, *On traces for* $\mathbf{H}(\mathbf{curl}, \Omega)$ *in Lipschitz domains*, J. Math. Anal. Appl. **276** (2002), no. 2, 845–867. MR1944792 ↑8

[BCS57] J. Bardeen, L. N. Cooper, and J. R. Schrieffer, *Theory of superconductivity*, Phys. Rev. **108** (1957), 1175–1204. ↑2

[BHvPS03] A. Buffa, R. Hiptmair, T. von Petersdorff, and C. Schwab, *Boundary element methods for Maxwell transmission problems in Lipschitz domains*, Numer. Math. **95** (2003), no. 3, 459–485. MR2012928 ↑4, 8, 24, 25

[BJOS13] S. Baldo, R. L. Jerrard, G. Orlandi, and H. M. Soner, *Vortex density models for superconductivity and superfluidity*, Comm. Math. Phys. **318** (2013), no. 1, 131–171. MR3017066 ↑4

[Bra94] E. H. Brandt, *Thin superconductors in a perpendicular magnetic ac field: General formulation and strip geometry*, Physical Review B **49** (1994), no. 13, 9024–9040. ↑4

[Bra96] E. H. Brandt, *Superconductors of finite thickness in a perpendicular magnetic field: Strips and slabs*, Physical Review B **54** (1996), no. 6, 4246–4264. ↑4

[BS08] S. C. Brenner and L. R. Scott, *The mathematical theory of finite element methods*, Third, Texts in Applied Mathematics, vol. 15, Springer, New York, 2008. MR2373954 ↑4

[BS21] T. Betcke and M. W. Scroggs, *Bempp-cl: A fast python based just-in-time compiling boundary element library.*, Journal of Open Source Software **6** (2021), no. 59, 2879. ↑5

[B$^+$19] S. Balay et al., *PETSc users manual*, Technical Report ANL-95/11, Revision 3.11, Argonne National Laboratory, 2019. ↑5

[CB05] J. R. Clem and E. H. Brandt, *Response of thin-film SQUIDs to applied fields and vortex fields: Linear SQUIDs*, Physical Review B **72** (2005), no. 17, 174511. ↑4

[EEK21] M. Elasmi, C. Erath, and S. Kurz, *The Johnson–Nédélec FEM–BEM coupling for magnetostatic problems in the isogeometric framework*, 2021. Available at arXiv:2110.04150. ↑13

[FHSS12] R. L. Frank, C. Hainzl, R. Seiringer, and J. P. Solovej, *Microscopic derivation of Ginzburg-Landau theory*, J. Amer. Math. Soc. **25** (2012), no. 3, 667–713. MR2904570 ↑2

[GL50] V. L. Ginzburg and L. D. Landau, *On the theory of superconductivity*, Zh. Eksp. Teor. Fiz. **20** (1950), 1064–1082. English translation in: *Collected papers of L.D.Landau*, Edited by D. Ter. Haar, Pergamon Press, Oxford 1965, pp. 546–568. ↑2

[Hac85] W. Hackbusch, *Multi-grid methods and applications*, Springer Series in Computational Mathematics, vol. 4, Springer-Verlag, Berlin, 1985. ↑5

[Hip02a] R. Hiptmair, *Finite elements in computational electromagnetism*, Acta Numer. **11** (2002), 237–339. MR2009375 ↑4

[Hip02b] R. Hiptmair, *Symmetric coupling for eddy current problems*, SIAM J. Numer. Anal. **40** (2002), no. 1, 41–65. MR1921909 ↑4, 24

[Kik87] F. Kikuchi, *Mixed and penalty formulations for finite element analysis of an eigenvalue problem in electromagnetism*, Proceedings of the first world congress on computational mechanics (Austin, Tex., 1986), 1987, pp. 509–521. MR912525 ↑5, 10

[KKGS03] M. M. Khapaev, M. Yu. Kupriyanov, E. Goldobin, and M. Siegel, *Current distribution simulation for superconducting multi-layer structures*, Superconductor Science and Technology **16** (2003), no. 1, 24–27. ↑4

[LL35] F. London and H. London, *The electromagnetic equations of the superconductor*, Proceedings of the Royal Society of London. Series A **149** (1935), 71–88. ↑2

[Lon50] F. London, *Superfluids*, Structure of matter series, Wiley, New York, 1950. ↑3, 22

[Mon03] P. Monk, *Finite element methods for Maxwell's equations*, Numerical Mathematics and Scientific Computation, Oxford University Press, New York, 2003. MR2059447 ↑4, 11, 14

[RBD02] P. Rosenbusch, V. Bretin, and J. Dalibard, *Dynamics of a single vortex line in a Bose-Einstein condensate*, Phys. Rev. Lett. **89** (2002), no. 20, 200403. ↑6, 21

[Rom19] C. Román, *On the first critical field in the three dimensional Ginzburg-Landau model of superconductivity*, Comm. Math. Phys. **367** (2019), no. 1, 317–349. MR3933412 ↑3, 6, 7, 17, 18

[RSS23] C. Román, E. Sandier, and S. Serfaty, *Bounded vorticity for the 3D Ginzburg-Landau model and an isoflux problem*, Proc. Lond. Math. Soc. (3) **126** (2023), no. 3, 1015–1062. MR4563866 ↑3, 6, 18

[RSS25] C. Román, E. Sandier, and S. Serfaty, *Vortex lines interaction in the three-dimensional magnetic Ginzburg–Landau model*, 2025. Available at arXiv:2510.14910. ↑3, 6

[SS11] S. A. Sauter and C. Schwab, *Boundary element methods*, Springer Series in Computational Mathematics, vol. 39, Springer-Verlag, Berlin, 2011. Translated and expanded from the 2004 German original. MR2743235 ↑4

[SS86] Y. Saad and M. H. Schultz, *GMRES: a generalized minimal residual algorithm for solving nonsymmetric linear systems*, SIAM J. Sci. Statist. Comput. **7** (1986), no. 3, 856–869. MR848568 ↑5

[Ste11] O. Steinbach, *A note on the stable one-equation coupling of finite and boundary elements*, SIAM J. Numer. Anal. **49** (2011), no. 4, 1521–1531. MR2831059 ↑13

Instituto de Ingeniería Matemática y Computacional & Facultad de Ciencias Biológicas, Pontificia Universidad Católica de Chile, Vicuña Mackenna 4860, 7820436 Macul, Santiago, Chile; and Centro de Modelamiento Matemático, Santiago, Chile.

Email address: `nicolas.barnafi@uc.cl`

Instituto de Ingeniería Matemática y Computacional, Pontificia Universidad Católica de Chile, Vicuña Mackenna 4860, 7820436 Macul, Santiago, Chile

Email address: `ignacio.labarca@uc.cl`

Facultad de Matemáticas & Instituto de Ingeniería Matemática y Computacional, Pontificia Universidad Católica de Chile, Vicuña Mackenna 4860, 7820436 Macul, Santiago, Chile

Email address: `carlos.roman@uc.cl`